

Periodic Modulation : Newly emergent emission behaviour in Pulsars

Rahul Basu^{1,2}, Dipanjan Mitra^{3,2}, Giorgi I. Melikidze^{2,4}

ABSTRACT

Periodic modulations are seen in normal period pulsars ($P > 0.1$ sec) over timescales ranging from a few seconds to several minutes. Such modulations have usually been associated with the phenomenon of subpulse drifting. A number of recent studies have shown subpulse drifting to exhibit very specific physical characteristics : i) drifting is seen only in conal components of the pulse profile and is absent in central core emission; ii) drifting pulsars are distributed over a narrow range of spin-down energy loss (\dot{E}), where pulsars with $\dot{E} < 2 \times 10^{32}$ erg s⁻¹ show this behaviour, iii) drifting periodicity (P_3) is anti-correlated with \dot{E} , such that pulsars with lower values of \dot{E} tend to have longer P_3 . These detailed characterisations of drifting behaviour on the other hand also revealed the presence of other distinct periodic modulations, which can be broadly categorised into two types, periodic nulling and periodic amplitude modulation. In contrast to drifting these periodic phenomena are seen across the entire profile in both the core and conal components simultaneously and are not restricted to any specific \dot{E} range. In this work we have assembled an exhaustive list of around 70 pulsars which show such periodic modulations, 22 of which were newly detected using observations from the Giant Meterwave Radio Telescope and the remaining compiled from past publications. The presence of such a significant group in the pulsar population suggests that periodic nulling and periodic amplitude modulations to be newly emergent phenomena in pulsars with their physical origin distinct from subpulse drifting.

Subject headings: pulsars: general — pulsars:

1. Introduction

Radio emission from normal period pulsars ($P > 0.1$ seconds) shows variations in their single pulses which exhibit different periodicities. Periodic behaviour over timescales of several hundred pulses is studied using longitude resolved fluctuation spectra (LRFS, Backer 1970a, 1973). LRFS requires single pulse sequence to be arranged in the form of a pulse stack, which is a two dimensional representation with pulse longitude along the abscissa and every subsequent period placed along the ordinate. Fourier transforms are carried out along each longitude range of the pulse stack to form LRFS. Single pulses are composed of one or more compo-

nents which are known as subpulses. Peak frequency in the fluctuation spectra represents periodicity of subpulse repetition at any given pulse longitude. Phase variations corresponding to the peak amplitude indicate the time delay with which subpulse appears with respect to a specific reference longitude.

Periodic modulations have been studied in great detail in the literature, with Ruderman & Sutherland (1975) suggesting subpulse drifting as primary mechanism for such variations. However, detailed phenomenological studies in recent past have revealed other likely sources for periodic behaviour in single pulses. We present a careful distinction between these possibilities in the discussion below.

1.1. Subpulse Drifting

The phenomenon of subpulse drifting is associated with systematic variations of subpulses within pulse window (Drake & Craft 1968). Detailed studies of subpulse drifting in a large number of pulsars (Rankin 1986; Gil & Sendyk 2000; Deshpande & Rankin 2001;

¹Inter-University Centre for Astronomy and Astrophysics, Pune, 411007, India, rahulbasu.astro@gmail.com.

²Janusz Gil Institute of Astronomy, University of Zielona Góra, ul. Szafrana 2, 65-516 Zielona Góra, Poland.

³National Centre for Radio Astrophysics, Tata Institute of Fundamental Research, Pune 411007, India.

⁴Evgeni Kharadze Georgian National Astrophysical Observatory, Abastumani, Georgia.

Weltevrede *et al.* 2006, 2007; Basu *et al.* 2016; Basu & Mitra 2018a; Basu *et al.* 2019a) reveal two important characteristics: evolution of drift pattern with line of sight (LOS) geometry, where the drifting is different for each component in profile, and dependence of drifting periodicity (P_3) on spin-down energy loss (\dot{E}).

Classification of profile types can be used to understand evolution of drifting with LOS geometry. Average radio emission beam is expected to consist of a central core component, surrounded by two concentric conal rings (Rankin 1990, 1993). The observed profile diversity is believed to be related to different LOS traverse across emission beam. When LOS cuts across edge of beam, conal Single (S_d) profiles are seen. As LOS traverses progressively more interior regions of beam, conal Double (D), conal Triple (${}_cT$) and conal Quadruple (${}_cQ$) profile classes are observed. Core dominated profiles, viz., core Single (S_t), core-cone Triple (T) and core-double cone Multiple (M) are expected to arise due to central LOS traverse of emission beam. In some pulsars with core emission, one of the conal pair is too weak to be detected and they are classified as $T_{1/2}$.

Subpulse drifting is a strictly conal phenomenon, with no drifting seen in core component (Rankin 1986). In addition, drifting behaviour also evolves from outer edge to central regions of emission beam. Systematic large scale phase variations are seen across entire profile in S_d and D profile classes. On the other hand phase variations for each conal component in ${}_cT$ and ${}_cQ$ profiles are usually different and show jumps and reversals from one component to another. In most M profiles drifting is largely phase stationary in outer conal components, but shows significant phase changes in inner cones (Basu *et al.* 2019a,b).

Subpulse drifting shows a clear dependence on \dot{E} , which is different from other periodic behaviour. Drifting is seen in pulsars with $\dot{E} < 5 \times 10^{32}$ erg s⁻¹. In addition, a correlation can also be inferred between drifting periodicity (P_3) and \dot{E} . If the periodicity measured in LRFS is not considered to be aliased, pulsars with low \dot{E} generally has longer P_3 than pulsars with higher \dot{E} . This anti-correlation becomes stronger under the assumption that subpulse motion is lagging behind co-rotation speed. In this scenario negative drifting with subpulse motion from trailing to leading edge of profile has $P_3 > 2P$, and positive drifting with subpulse motion towards trailing edge has $P < P_3 < 2P$. The estimated dependence is given as $P_3 \propto \dot{E}^{-0.6 \pm 0.1}$ (Basu *et al.* 2016).

Subpulse drifting is associated with non-stationary plasma flow in Inner Acceleration Region (IAR) of pulsars, which is best explained using a partially screened gap model (PSG, Gil *et al.* 2003; Szary *et al.* 2015). PSG model considers a steady flow of ions from stellar surface which screens the electric field in IAR by a screening factor (η):

$$\eta = 1 - \rho_i / \rho_{GJ}; \quad \rho_{GJ} = \vec{\Omega} \cdot \vec{B} / 2c. \quad (1)$$

Here, ρ_i is density of ions and ρ_{GJ} the Goldreich-Julien density (Goldreich & Julian 1969). The plasma responsible for radio emission is generated in IAR in the form of sparking discharges (Ruderman & Sutherland 1975). Sparks do not co-rotate with the star, but lag behind co-rotation speed which results in subpulse drifting.

In presence of PSG the drift speed of sparks (v_{sp}) can be expressed as (Basu *et al.* 2016):

$$v_{sp} = \eta(E/B)c, \quad (2)$$

where B is magnetic field and E is co-rotation electric field. The subpulses can be associated with spark motion in IAR. It is speculated that IAR is packed with circular sparks which are also equidistant, represented by size h (Gil & Sendyk 2000). The time of repetition of sparks at any longitude, which is also drifting periodicity (P_3), is estimated as

$$P_3 = 2h/v_{sp}. \quad (3)$$

When η is small ($\eta \sim 0.1$) it can be shown that P_3 in PSG is estimated as (Szary 2013):

$$P_3 = \frac{1}{2\pi\eta\cos\alpha}, \quad (4)$$

where α is inclination angle between rotation and magnetic axes. The anti-correlation between P_3 and \dot{E} can be derived from eq.(3) and eq.(4) using basic physical approximations. When the full energy outflow from polar cap is associated with \dot{E} using factor ξ we obtain (Basu *et al.* 2016):

$$P_3 = 2 \times 10^{-9} \left(\frac{\gamma_0}{\xi} \right) \left(\frac{\dot{E}}{\dot{E}_1} \right)^{-0.5}, \quad (5)$$

where $\gamma_0 \sim 10^6$ is Lorentz factor of primary particles in IAR, $\xi \sim 10^{-3} - 10^{-4}$ is scaling factor obtained from the fraction of non-thermal X-ray emission (Becker 2009), and $\dot{E}_1 = 4 \times 10^{31}$ erg s⁻¹.

1.2. Other Periodic Modulations

Recent studies have revealed presence of additional periodic behaviours seen in fluctuation spectra, which include periodic nulling (Herfindal & Rankin 2007) and periodic amplitude modulation. Periodic nulling is seen in conal as well as core-cone profiles, where the core components also vanishes along with cones in a periodic manner. This prompted Basu *et al.* (2017) to identify periodic nulling to be a different phenomenon. In addition certain pulsars with core emission show low frequency modulation in intensity, where the core component also participates (Basu *et al.* 2016; Mitra & Rankin 2017). This behaviour is known as periodic amplitude modulation.

There are clear differences between physical parameters of subpulse drifting and other periodic modulations. A significant number of pulsars showing this behaviour have high \dot{E} in excess of 5×10^{32} erg s^{-1} . Periodic nulling and periodic amplitude modulation are usually seen as low frequency features in fluctuation spectra. The corresponding longer periodicities are not correlated with \dot{E} unlike subpulse drifting.

Contrasting behaviour of drifting and other periodic modulations are clearly illustrated in pulsars where both effects are seen in pulse sequence (Basu *et al.* 2017, 2019a). In all such cases the low frequency feature in fluctuation spectra can be identified as periodic modulation. One example is the pulsar B2003–08, with a M type profile, which has subpulse drifting and periodic nulling. Subpulse drifting is seen only in conal pairs, where the outer pairs have phase stationary behaviour and the inner pairs exhibit large scale bi-drifting behaviour. Periodic nulling is seen across entire profile as a phase stationary behaviour (Basu *et al.* 2019b). Another pulsar B1737+13, with M type profile, shows presence of both subpulse drifting and periodic amplitude modulation. Drifting only affects the conal components, but amplitude modulation is seen across all components (Force & Rankin 2010).

Physical mechanism of periodic modulations is still unknown, but is expected to be different from subpulse drifting. Subpulse drifting can be explained using standard physics of non-stationary flow in the PSG as explained above. On the other hand origin of a number of other physical phenomena in pulsar radio emission cannot be explained using this standard model. In certain pulsars subpulses show presence of quasi-periodic structures which are also called microstructures. They likely originate due to temporal modulations of non-

stationary plasma flow resulting in alternating radial emitting regions interspersed with relatively less bright parts (Mitra *et al.* 2015). However, presence of such modulations require variations in the plasma generation process in PSG, which are currently unknown.

Pulsar radio emission also shows the presence of nulling (Backer 1970b), and mode changing (Backer 1970c), where emission switches from one steady state to another. These phenomena are not periodic, with rapid transition between different states (usually within a period), which switch back to the initial state after irregular intervals. A notable exception is the periodic swooshing events in pulsars B0919+06 and B1859+07 (Rankin *et al.* 2006; Wahl *et al.* 2016). Their physical origin, unlike drifting, also cannot be explained using the steady state conditions in IAR, and requires changes in plasma generation process which are still unexplored.

A detailed classification of subpulse drifting from a complete list of pulsars has been reported in Basu *et al.* (2019a). However, no equivalent study exists for periodic nulling and periodic amplitude modulation, which we plan to address in this work. We have carried out measurements of nulling and periodicities in a large number of pulsars, observed using the Giant Meter-wave Radio Telescope (GMRT), as well as conducted an exhaustive literature survey. In section 2 we describe details of observations from GMRT as well as analysis schemes used to determine nulling and periodic behaviour. Section 3 carries out a collective study of all known pulsars showing periodic modulations, including those previously reported in literature. A detailed discussion comparing physical properties of different periodic behaviours in pulsars is presented in section 4. Finally, section 5 summarizes primary results and conclusions of our studies.

2. Observations and Analysis

A large sample of pulsars was assembled by Basu *et al.* (2019a) to study drifting behaviour in the population. This list included more than thirty pulsars observed with GMRT and another fifty from archival observations (Mitra & Rankin 2011). Many of these sources exhibited nulling and periodic modulations, whose properties we have explored in this work. We have carried out detailed nulling and fluctuation spectral analysis of 62 pulsars as shown in Table 1.

Pulsars were observed in ‘Phased-Array’ mode at 325 MHz frequency band. We analysed sources with-

out any previous studies of nulling or periodic modulation. Details of observations as well as instrumental setup are available in Basu *et al.* (2019a). Initially, recorded signals from each pulsar were converted into well calibrated, baseline corrected, single pulse sequence (Mitra *et al.* 2016; Basu *et al.* 2016). Subsequently, number of different analyses were carried out, which are briefly summarized below (Basu *et al.* 2017).

Nulling was studied by identifying suitable on and off-pulse windows in profile. Average energies in these windows were calculated for each pulse. Pulse energy distribution for the entire sequence was estimated to search for presence of nulling. Figure 1 shows an example of on and off-pulse energy distributions for the nulling pulsar B0138+59. On-pulse energies show bimodal behaviour where null pulses are coincident with off-pulse distribution. Nulling fraction (NF) was estimated by fitting Gaussian functions to null and the off-pulse distributions and finding suitable scaling relation between them (Ritchings 1976). Error in NF was calculated from statistical errors of functional fits. In a few pulsars there were short duration (a few periods), infrequent, but clear nulls, which were too few to resemble fully formed Gaussian functions. In such cases the number of null pulses were individually counted to estimate NF. Error in NF was estimated as $\delta\text{NF} = \sqrt{n_p}/N_p$, where n_p corresponded to all null pulses and N_p is total number of pulses.

In Table 1 we report 20 pulsars where nulling was present. 19 pulsars in the list show clear separation between on and off-pulse distributions, indicating absence of nulling. Last column in the Table identifies 17 pulsars without any nulling. In addition, two pulsars B0450–18 and B1642–03 also had no detectable nulls. Detection sensitivities of single pulses in remaining 23 pulsars were not sufficient to rule out presence of nulling. Figure 2 shows an example of null length and burst length distributions for the pulsar B0138+59. There were 17 pulsars where such distributions could be estimated. The Table also lists total number of transitions from null to burst sequence (N_T) as well as average duration of nulls ($\langle NL \rangle$) and bursts ($\langle BL \rangle$) in these 17 pulsars.

We have also investigated the presence of periodic modulations in these pulsars. This involved determining time variations in LRFS as well as harmonic resolved fluctuation spectra (HRFS, Deshpande & Rankin 2001), as described in Basu *et al.* (2016). In nulling pulsars, with well defined null and burst pulses, pres-

ence of periodic nulling was also explored. Nulls were identified as ‘0’ and bursts as ‘1’ and Fourier transforms of this binary series was determined (see Basu *et al.* 2017, for details). Figure 3 shows time varying LRFS and nulling FFT in the pulsar J1857–1027 with periodic nulling.

Periodic modulations were detected in 24 pulsars, where 11 pulsars exhibited periodic nulling and another 6 showed periodic amplitude modulations. Exact nature of periodic behaviour in remaining 7 pulsars was indeterminate due to lower sensitivity of detections. Only 10 out of 17 pulsars with clearly separated null and burst pulses had periodic nulling. Additionally, the pulsar J1857–1027 showed presence of clear nulls of 5-10 P durations which were also periodic in nature (see figure 3), but the emission was too weak for other nulling analysis. Table 1 reports peak modulation frequency (f_p), width of peak feature (FWHM), strength of the feature (S_M), defined as relative height of feature from baseline divided by FWHM, and periodicity (P_M). Error in estimating peak frequency is given as $\delta f_p = \text{FWHM}/2\sqrt{2\ln(2)}$ (Basu *et al.* 2016).

3. Pulsars with Periodic Modulations

We have investigated all known pulsars with periodic modulations which are different from subpulse drifting. There are around 70 pulsars exhibiting periodic behaviour either in the form of periodic nulling, periodic amplitude modulations or indeterminate cases. Individual pulsars belonging to each group are described below along with their basic physical properties.

3.1. Periodic Nulling

Table 2 presents twenty nine pulsars which show presence of periodic nulling. The Table also describes various physical characteristics of these pulsars including their \dot{E} values, nulling periodicity (P_N), profile classification, presence of subpulse drifting and/or mode changing in pulse sequence, and references for initial detection of periodic nulling in each pulsar. Periodic nulling was first detected in the pulsar B1133+16 by Herfindal & Rankin (2007) and subsequently its presence was reported in PSR J1819+1305 by Rankin & Wright (2008). Detailed work of Herfindal & Rankin (2009) identified additional 9 pulsars to show this behaviour, which was further increased to a total of 19 pulsars by Basu *et al.* (2017, see Table 3 of this paper). Subsequently, pe-

TABLE 1
ESTIMATIONS OF NULLING AND MODULATION PERIODICITY

PSR	P (s)	N_p	NF (%)	N_T	$\langle BL \rangle$ (P)	$\langle NL \rangle$ (P)	f_p (cy/P)	FWHM (cy/P)	S_M (P/cy)	P_M (P)	Remarks
B0105+65	1.284	3020	No Nulls
B0138+59	1.223	1960	7.6±1.0	89	19.0	2.8	0.023±0.017	0.040	21.2	44±30	Periodic Nulls
B0320+39	3.032	2073	0.7±0.2	14	140.4	1.0	Short Nulls
B0355+54	0.156	13113	Low emission
B0402+61	0.595	3041	No Nulls
J0421-0345	2.161	1226	Low emission
B0447-12	0.438	2742	No Nulls
B0450-18	0.549	2738	0.064±0.023	0.055	18.1	15.6±5.7	Amp. Mod.
B0450+55	0.341	2658	0.111±0.016	0.037	27.4	9.0±1.3	Amp. Mod.
B0523+11	0.354	3436	No Nulls
B0559-05	0.396	3900	No Nulls
B0609+37	0.444	2049	Low emission
B0621-04	1.039	1357	0.0137±0.0003	0.0007	313.5	73.1±1.6	Low emission
B0727-18	0.510	3537	Low emission
B0740-28	0.167	3629	No Nulls
B0809+74	1.292	890	1.2±0.4	6	145.2	2.0	Short Nulls
B0818-13	1.238	2425	0.9±0.1	16	130.6	1.3	Short Nulls
B0820+02	0.865	1376	0.5±0.2	7	181.1	1.0	Short Nulls
B0905-51	0.254	2358	No Nulls
B0906-17	0.402	2244	12.4±1.1	Low emission
B0919+06	0.431	4100	No Nulls
B0932-52	1.445	1614	1.9±0.1	30	48.7	1.5	0.029±0.016	0.038	7.6	35±19	Periodic Nulls
B1112+50	1.656	1977	34.8±1.4	215	3.4	5.8	Med. Nulls
B1237+25	1.382	946	8.9±1.0	40	21.2	2.1	0.039±0.007	0.018	39.4	25.7±4.9	Periodic Nulls
B1322+83	0.670	2672	Low emission
B1508+55	0.740	1784	5.2±0.4	95	16.7	2.0	0.066±0.032	0.076	2.6	15.1±7.3	Periodic Nulls
B1510-48	0.455	2104	0.027±0.003	0.007	57.9	36.6±4.1	Low emission
B1540-06	0.709	5660	No Nulls
B1541+09	0.748	3035	0.066±0.021	0.050	6.2	15.1±4.8	Amp. Mod.
B1556-44	0.257	3550	No Nulls
B1601-52	0.658	4551	0.047±0.015	0.036	1.7	21.4±7.0	Low emission
B1604-00	0.422	3248	0.15±0.07	0.029±0.011	0.026	11.9	34±13	Amp. Mod.
B1612+07	1.207	914	Low emission
B1642-03	0.388	1502	0.078±0.032	0.075	5.9	12.8±5.2	Amp. Mod.
J1650-1654	1.750	2162	0.016±0.011	0.026	5.1	64±45	Low emission
B1700-18	0.804	1849	0.023±0.009	0.021	8.9	43±15	Low emission
B1717-29	0.620	1850	No Nulls
B1718-02	0.478	3075	Low emission
B1742-30	0.367	1900	Low emission
B1804-08	0.164	1700	Low emission
B1822-09	0.769	2328	No Nulls
B1831-04	0.290	2000	Low emission
B1845-19	4.308	2223	27.2±1.7	410	3.4	2.0	Short Nulls
B1851-14	1.147	1024	Low emission
J1857-1027	3.687	1000	>30	0.056±0.033	0.077	11.2	18±10	Periodic Nulls
B1857-26	0.612	1955	4.3±0.5	198	8.6	1.2	Short Nulls
B1905+39	1.236	1124	10.0±0.5	80	11.5	2.3	0.021±0.011	0.026	26.9	47±24	Periodic Nulls
B1907-03	0.505	1279	No Nulls
B1929+10	0.227	1824	0.088±0.006	0.014	33.0	11.4±0.8	Amp. Mod.
B1937-26	0.403	1904	Low emission
B1952+29	0.427	3512	0.039±0.018	0.042	1.9	26±12	Low emission
B2016+28	0.558	5358	No Nulls
B2021+51	0.529	5598	0.045±0.030	0.070	5.5	22±15	Low emission
B2043-04	1.547	1980	No Nulls
B2045-16	1.962	1199	9.2±0.7	69	14.4	2.8	0.023±0.013	0.031	25.5	43±25	Periodic Nulls
B2053+21	0.815	2198	No Nulls
B2111+46	1.015	2000	8.7±0.5	130	11.1	4.1	0.021±0.005	0.011	70.4	48±10	Periodic Nulls
B2217+47	0.538	2179	No Nulls
B2224+65	0.683	2049	Low emission
B2310+42	0.349	3583	5.1±0.8	54	36.6	2.9	0.045±0.015	0.034	11.4	22.3±7.2	Periodic Nulls
B2319+60	2.256	2121	15.2±1.1	100	15.0	6.2	0.017±0.005	0.012	39.6	58±17	Periodic Nulls
B2327-20	1.644	1854	10.7±1.0	130	11.9	2.3	0.048±0.023	0.054	13.3	20.8±9.9	Periodic Nulls

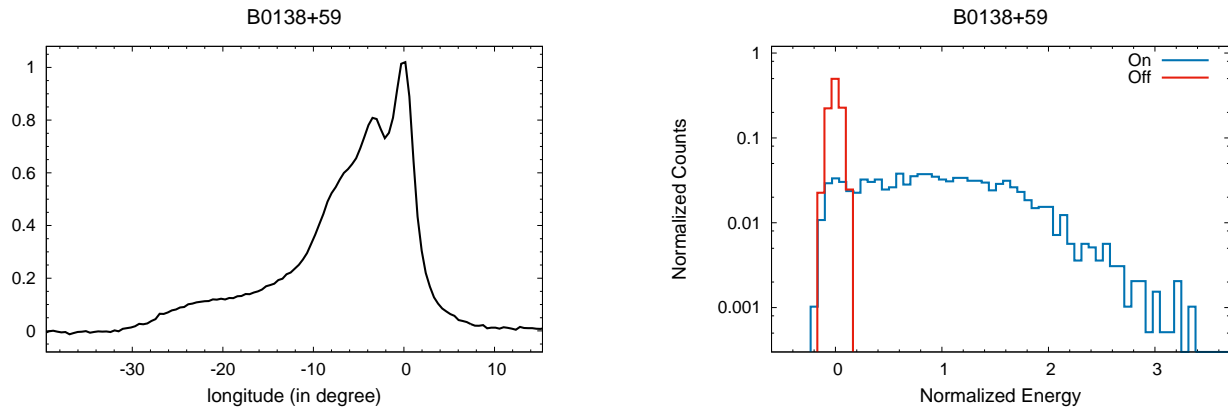


Fig. 1.— The figure shows average profile (left panel) and pulse energy distribution (right panel) of the pulsar B0138+59. (The complete figure set (62 images) is available.)

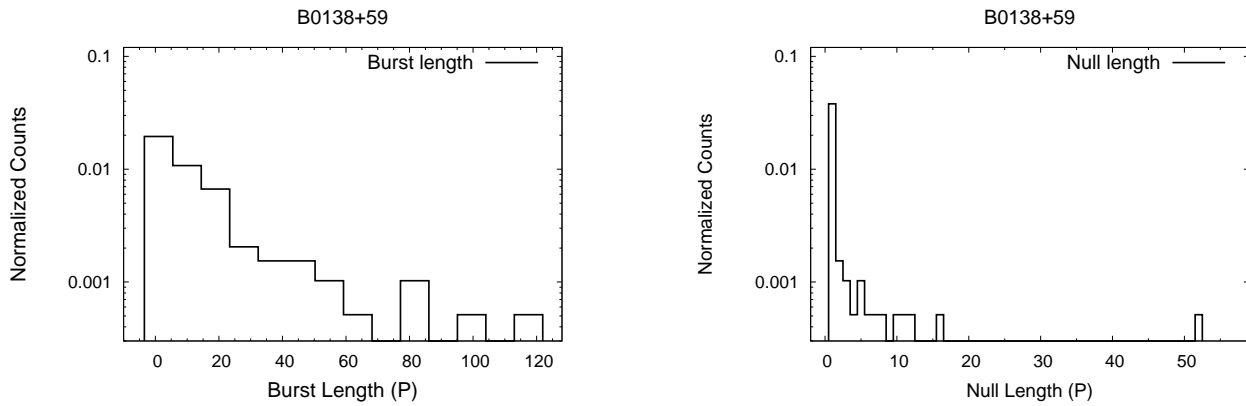


Fig. 2.— Burst length (left panel) and Null length (right panel) distributions of the pulsar B0138+59. (The complete figure set (17 images) is available.)

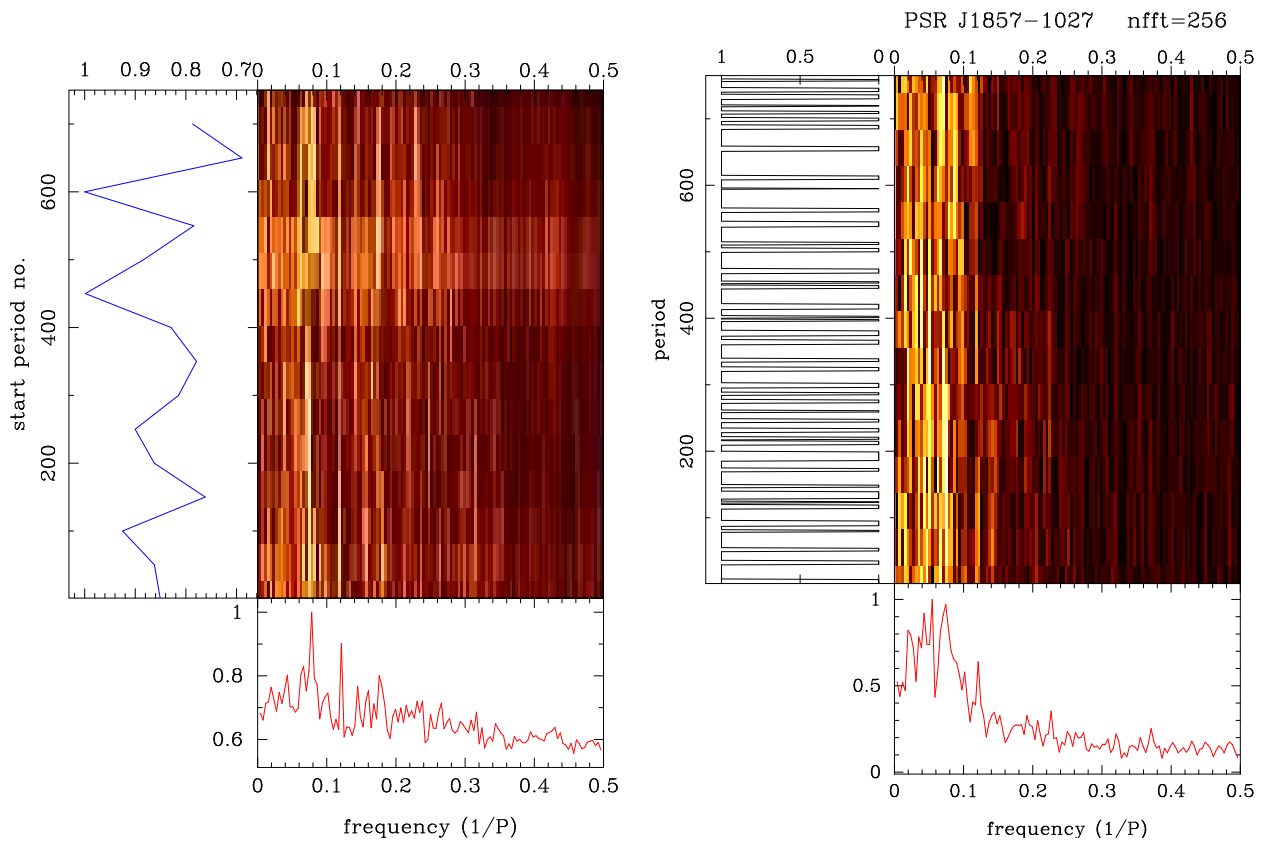


Fig. 3.— Time evolution of LRFS (left panel) and Null-Burst time series FFT (right panel) in the pulsar J1857–1027. (The complete figure set (24 images) is available.)

Table 2: Periodic Nulling

PSR	\dot{E} (2×10^{32} erg/s)	P_N (P)	Profile		REF
B0031–07	0.096	75±14	S_d	Drift, Mode	[1]
B0138+59	0.042	44±30	M	...	[2]
B0301+19	0.096	103±34	D	Drift	[3]
B0525+21	0.151	46±4	D	...	[3]
B0751+32	0.071	73±10	D	...	[3]
B0823+26	2.260	14±3	S_t	Mode	[4]
B0834+06	0.650	16±4	D	Drift	[3]
B0932–52	0.305	35±19	S_d	Drift	[2]
B1133+16	0.440	29±2	D	...	[5]
B1237+25	0.072	26±5	M	Drift, Mode	[2]
B1508+55	2.440	15±7	T	...	[2]
J1649+2533	0.106	27±2	[3]
B1706–16	4.470	130±70	S_t	...	[1]
J1727–2739	0.101	206±33	D	Drift	[1]
B1738–08	0.053	34±8	$cQ?$	Drift	[1]
J1819+1305	0.060	64±8	cQ	...	[6]
B1819–22	0.041	134±33	D	Drift, Mode	[7]
J1857–1027	0.042	18±10	T	...	[2]
B1905+39	0.057	47±24	M	...	[2]
B1918+19	0.320	85±14	cT	Drift, Mode	[3]
B1944+17	0.056	600±52	cT	Drift, Mode	[1]
B2003–08	0.046	41±4	M	Drift, Mode	[8]
B2034+19	0.045	57±6	T	...	[3]
B2045–16	0.287	51±20	T	Drift	[1]
B2111+46	0.135	48±10	T	...	[2]
B2303+30	0.146	43±8	S_d	Drift, Mode	[3]
B2310+42	0.520	32±11	cT	Drift	[1]
B2319+60	0.121	58±17	cQ	Drift, Mode	[2]
B2327–20	0.206	19±1	T	...	[1]

1-Basu *et al.* (2017); 2-This paper; 3-Herfindal & Rankin (2009); 4-Basu & Mitra (2019); 5-Herfindal & Rankin (2007); 6-Rankin & Wright (2008); 7-Basu & Mitra (2018b); 8-Basu *et al.* (2019b).

riodic nulling was also detected in PSR B0823+26 (Basu & Mitra 2019), PSR B1819–22 (Basu & Mitra 2018b) and PSR B2003–08 (Basu *et al.* 2019b). We have identified an additional 8 pulsars which exhibit periodic nulling in Table 1.

Physical characteristics of these pulsars indicate that periodic nulling coexists with subpulse drifting and mode changing. In this list there are 15 pulsars which show subpulse drifting and 9 pulsars also has presence of multiple emission modes. In 8 pulsars all three phenomena are seen in the same pulse sequence. Profile classification shows that periodic nulling is not restricted to any particular profile type but seen across all classes; $S_d = 3$; $S_t = 2$; $D = 7$; ${}_cT = 3$; ${}_cQ = 3$; $T = 6$; $M = 4$; not classified = 1.

3.2. Periodic Amplitude Modulation

We have identified eighteen pulsars with periodic amplitude modulation which are reported in Table 3. The Table also describes different physical characteristics of each pulsar including \dot{E} , modulation periodicity (P_A), profile classification, and presence of subpulse drifting and/or mode changing. These periodicities were measured in the works of Weltevrede *et al.* (2006, 2007); Basu *et al.* (2016) and this work, but they were not recognised as a separate phenomenon in previous studies.

Some of the interesting physical behaviour of periodic amplitude modulation are summarized below. The pulsar B0823+26 has periodic amplitude modulation during its B mode, while the Q mode shows periodic nulling (Basu & Mitra 2019). The two modes in PSR B1822–09 have periodic amplitude modulation with different periodicities (Latham *et al.* 2012; Hermsen *et al.* 2017; Yan *et al.* 2019). PSR B1737+13 shows drifting in its conal components (Force & Rankin 2010). Periodic amplitude modulation is seen primarily in profiles with central LOS traverse, where usually prominent core emission is present. The number of pulsars belonging to different profile types are estimated to be $S_t = 3$; ${}_cT = 1$; $T_{1/2} = 2$; $T = 10$; $M = 1$; not classified = 1.

3.3. Unresolved Modulation

Twenty four pulsars show clear periodicities in their single pulse sequence, but their detection sensitivities are insufficient to determine the exact nature of modulation. Table 4 shows basic physical properties of these pulsars including \dot{E} , modulation periodicity

(P_M), profile classification, and presence of subpulse drifting. Mode changing is not seen in any of these sources. Four pulsars in this group, PSR B0621–04, B1510–48, J1650–1654 and B1700–18 also has subpulse drifting. Their profiles show a wide variety with $S_t = 7$; $D = 4$; ${}_cQ = 1$; $T_{1/2} = 3$; $T = 1$ or 2 ; $M = 1$ or 2 ; not classified = 6.

There are another additional twenty to thirty pulsars where periodic behaviour was also reported in earlier works (Weltevrede *et al.* 2006, 2007). In eight of them, PSR B0329+54, B0402+61, B0919+06, B0950+08, B1112+50, B1612+07, B1937–26 and B2217+47 we did not find any clear modulation features in fluctuation spectra. In the remaining cases more sensitive observations are required to validate presence of periodic behaviour.

4. Periodic Modulation : Distinct physical phenomenon

Major differences between periodic modulations and subpulse drifting are summarized in Table 5. We have estimated dependence of modulation periodicity (P_M) with \dot{E} which is shown in figure 4. The figure represents P_M of three groups, periodic nulling (black open circles), periodic amplitude modulation (blue rhombus) and indeterminate periodic modulation (green square), defined in the previous section, along \dot{E} axis. Drifting periodicities (red filled circles) are also shown for comparisons. The figure highlights two primary features, a clear distinction between subpulse drifting and other periodic modulations, and overlapping behaviour between the three groups of periodic modulations.

Physical differences between subpulse drifting and other periodic modulations are also seen in their distributions of periodicity and \dot{E} . Periodic modulations (figure 5, left panel) have typical periodicities between 10-200 P , the distribution peaking around 50 P , and there are very few exceptions, around five cases, outside this range. On the other hand subpulse drifting has periodicity below 20 P in most cases, with the distribution peaking around 5 P . Longer periodic drifting is usually seen for low \dot{E} pulsars. One of the primary limitations of measuring periodic phenomena in pulsars, particularly short periodicities, is the aliasing effect around 2 P . This is reflected in the sharp cutoff at lower part of drifting periodicity distribution, possibly skewing it towards longer periodicities. \dot{E} distributions (figure 5, right panel) of the two populations

Table 3: Periodic Amplitude Modulation

PSR	\dot{E} (2×10^{32} erg/s)	P_A (P)	Profile	
B0450-18	6.850	16 ± 6	T	...
B0450+55	11.850	9 ± 1	T	...
B0823+26	2.260	6 ± 1	S_t	Mode
B1055-52	150.500	21 ± 2
B1541+09	0.204	15 ± 5	T	...
B1600-49	5.750	50 ± 26	T	...
B1604-00	0.805	34 ± 13	T	...
B1642-03	6.050	13 ± 4	S_t	...
B1718-32	1.175	23 ± 9	$T_{1/2}$...
B1732-07	3.250	20 ± 8	T	...
B1737+13	0.555	~ 90	M	Drift
B1737-39	2.835	10 ± 4	T	...
B1745-12	3.910	7 ± 1	T	...
B1822-09	22.800	46 ± 1	$T_{1/2}$	Mode
B1845-01	3.615	20 ± 8	cT	...
B1917+00	0.735	11 ± 0.4	T	...
B1929+10	19.650	12 ± 1	S_t	...
B1946+35	3.775	50 ± 10	T	...

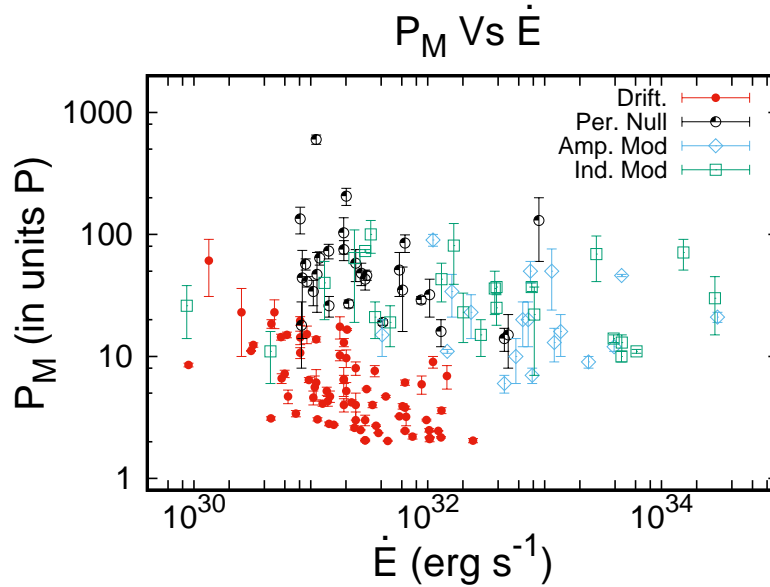


Fig. 4.— The figure shows modulation periodicities (P_M) of pulsars represented along with their spin-down energy loss (\dot{E}). Periodic nulling (black open circles), periodic amplitude modulation (blue rhombus) and indeterminate periodic modulations (green square) are shown in the figure, along with subpulse drifting (red filled circles) for comparison. The three periodic modulations overlap along \dot{E} axis, underlying their common physical origin. Subpulse drifting on the other hand has different physical behaviour. It is seen for a limited region along \dot{E} axis ($\leq 2 \times 10^{32}$ erg s⁻¹) and is weakly anti-correlated with \dot{E} .

Table 4: Periodic Modulation (Unresolved)

PSR	\dot{E} (2×10^{32} erg/s)	P_M (P)	Profile	
B0621-04	0.146	73±2	M	Drift
B0756-15	1.005	23±10	T _{1/2}	...
B1114-41	1.87	36±14	S _t	...
B1510-48	1.94	37±4	...	Drift
J1603-2531	13.85	69±28	S _t	...
B1601-52	0.178	21±7	D	...
J1650-1654	0.118	64±45	D	Drift
B1700-18	0.655	43±15	...	Drift
B1702-19	30.55	11±0.4	T _{1/2}	
B1730-37	77.0	71±20	...	
B1753+52	0.023	11±5	_c Q	...
B1758-03	0.835	81±42	T _{1/2}	...
B1839+56	0.066	40±20
B1839+09	3.88	37±3	S _t	...
B1859+01	19.45	14±1	T	...
B1907+10	22.85	13±2	S _t	...
B1911-04	1.425	15±5	S _t	...
B1952+29	0.004	26±12	M/T?	...
B1953+50	1.94	25±7	S _t	...
B2011+38	143.0	30±15
B2021+51	4.08	22±15	D	...
B2106+44	0.239	19±7
B2255+58	22.75	10±1	S _t	...
J2346-0609	0.163	100±30	D	...

Table 5: Comparing Periodic Behaviour in Pulsar Radio Emission

	Subpulse Drifting	Periodic Modulations
Profile Component	(i) Only seen in conal components. (ii) Different phase variations for different components.	(i) Simultaneously seen in central core and cones. (ii) longitude stationary, similar across all components.
Spindown Energy	(i) Seen in pulsars with $\dot{E} < 5 \times 10^{32}$ erg s ⁻¹ . (ii) P_3 weakly anti-correlated with \dot{E} .	(i) Seen in pulsars with wide \dot{E} distribution. (ii) $P_M \sim 10-200P$, no dependence of P_M on \dot{E} .
Origin	(i) Localised in Inner Acceleration Region. (ii) Associated with sparking process of plasma generation.	(i) Seen in both poles of pulsars with interpulse emission. (ii) Largescale variations affecting pulsar magnetosphere.

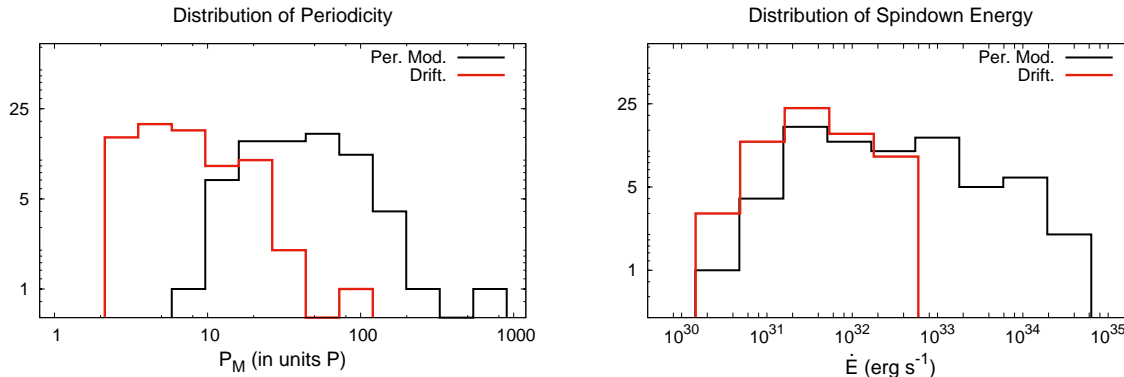


Fig. 5.— The figure shows distributions of modulation periodicity (left panel) and spin-down energy loss (right panel) for subpulse drifting and other periodic modulations. A clear distinction is seen between the two populations in both plots. Subpulse drifting is seen in pulsars with $\dot{E} < 2 \times 10^{32} \text{ erg s}^{-1}$, while periodic modulations are seen along a wider \dot{E} range. Subpulse drifting has usually lower periodicities with only a small fraction exceeding $20P$. On the other hand modulation periodicities are usually longer with typical values between 10 and $200P$.

also show very different behaviours. Subpulse drifting peaks around $3 \times 10^{31} \text{ erg s}^{-1}$ with an upper cutoff around $2 \times 10^{32} \text{ erg s}^{-1}$. In contrast periodic modulations are seen over a much wider \dot{E} range, with a plateau between 10^{31} and $10^{34} \text{ erg s}^{-1}$.

Both periodic nulling and periodic amplitude modulation share a number of identical features. This include lack of any dependence of their periodicities on \dot{E} , presence across the entire profile including core emission, and longitude stationary behaviour in all components. These suggest that their underlying physical processes are also likely to be similar. We propose that they represent a class of newly emergent emission behaviour in pulsars with distinct physical mechanism compared to subpulse drifting.

We have also compared physical properties of pulsars with periodic nulling and general nulling population. A detailed literature survey of nulling is reported in Table 6, which lists pulsar names, \dot{E} , nulling fraction (NF), reference for NF, and profile type. Only traditional nulling pulsars are considered for comparisons and more extreme examples like intermittent pulsars are not included. We have also excluded sources where only the upper limits of NF are reported due to lower sensitivity detections. This left eighty three pulsars where nulling is unambiguously observed.

No clear trends emerge for nulling, either in NF or their profile types. \dot{E} distribution of all nulling pulsars is shown in figure 6 along with the distribution

for periodic nulling. There is no sharp cutoff seen in the \dot{E} distributions, unlike subpulse drifting. However, nulling becomes less prevalent in high \dot{E} pulsars, with no nulling seen above $10^{34} \text{ erg s}^{-1}$. The figure also shows that distribution of periodic nulling pulsars cannot be distinguished from the non-periodic case.

It is likely that periodic nulling is more prevalent than the twenty nine cases reported here, and more sensitive single pulse studies in future will increase this number. For example, in three pulsars B1114–41, B1758–03 and J2346–0609 presence of periodic behaviour is seen in fluctuation spectra, but detection sensitivity of single pulses were not sufficient to ascertain periodic nulls. However, there are also several examples where sensitive single pulse studies could not detect presence of any periodicity associated with nulling. We did not detect periodicity in seven out of possible seventeen pulsars studied here. Basu *et al.* (2017, see Table 2) also reported eight pulsars without any periodic nulling, despite sensitive single pulse detections. Currently, periodic nulling is seen in around 35% of nulling pulsars.

5. Summary and Conclusion

In this paper we have carried out a detailed study of periodic amplitude modulation and periodic nulling seen in single pulse sequence of many normal period ($P > 0.1 \text{ s}$) pulsars. A complete list of all possible

TABLE 6
NULLING IN PULSARS

PSR	\dot{E} (2×10^{32} erg/s)	NF (%)	Profile	REF	PSR	\dot{E} (2×10^{32} erg/s)	NF (%)	Profile	REF
B0031–07	0.096	37.7	S_d	[1]	B1738–08	0.053	15.8±1.4	cQ	[5]
B0045+33	0.258	21	...	[2]	B1742–30	42.45	32.5±1.2	M	[5]
B0138+59	0.042	7.6±1.0	M	[3]	B1747–46	0.625	2.4±0.5	S_t	[5]
B0301+19	0.096	7.4±0.7	D	[4]	J1752+2359	1.855	75	...	[15]
B0320+39	0.005	0.7±0.2	cT	[3]	B1749–28	0.009	1.0±0.4	T	[5]
B0525+21	0.151	28±2	D	[4]	B1758–03	0.835	26.9±1.6	T	[5]
B0628–28	0.73	13.6±1.9	S_d	[5]	J1808–0813	0.364	10.8±1.1	S_d	[5]
B0751+32	0.071	38±6	D	[4]	B1809–173	2.15	5.8±4	S_t	[10]
B0809+74	0.015	1.2±0.4	S_d	[3]	B1813–36	6.95	16.7±0.7	T	[5]
B0818–13	0.219	0.9±0.1	S_d	[3]	J1819+1305	0.060	41±6	cQ	[4]
B0820+02	0.032	0.5±0.2	S_d	[3]	J1820–0509	4.795	67±3	...	[10]
B0823+26	2.26	3.85±0.05	S_t	[6]	B1819–22	0.041	5.5±0.2	D	[16]
B0834+06	0.65	4.4±0.4	D	[5]	J1831–1223	0.046	4±1	...	[10]
B0906–17	2.04	12.4±1.1	T	[3]	J1840–0840	0.031	50±6	D	[17]
J0930–2301	0.113	>30	...	[7]	B1845–19	0.058	27.2±1.7	T	[3]
B0932–52	0.305	1.9±0.1	S_d	[3]	B1848+12	1.30	51±2	S_t	[4]
B0940–55	15.4	<12.5	S_t	[8]	J1857–1027	0.042	> 30	T	[3]
B0940+16	0.014	8±3	T	[9]	B1857–26	0.176	4.3±0.5	M	[3]
B0942–13	0.048	14.4±0.9	$T_{1/2}$	[5]	J1901–0906	0.057	3.8±0.7	D	[5]
J1049–5833	0.082	47±3	...	[10]	B1905+39	0.057	10.0±0.5	M	[3]
B1112+50	0.109	34.8±1.4	$T_{1/2}$	[3]	B1907+03	0.070	4±0.2	T/M	[9]
B1114–41	1.87	3.3±0.5	S_t	[5]	J1920+1040	0.118	50±4	...	[10]
B1133+16	0.440	13±2	D	[5]	B1918+19	0.320	2.0±0.3	cT	[5]
B1237+25	0.072	2.5±0.1	M	[5]	J1926–1314	0.063	74±2	...	[18]
B1322–66	6.55	9.1±3	...	[10]	B1942+17	0.018	60	D	[19]
B1325–49	0.037	4.2±0.3	M	[5]	B1942–00	0.093	21±1	D	[9]
B1358–63	5.50	1.6±1	...	[10]	B1944+17	0.056	32.0±1.6	cT	[5]
J1502–5653	2.35	93±4	...	[10]	B2003–08	0.046	28.6±3.4	M	[20]
B1508+55	2.44	5.2±0.4	T	[3]	B2034+19	0.045	44±4	T	[4]
J1525–5417	3.085	16±5	...	[10]	B2045–16	0.287	8.8±0.6	T	[5]
B1524–39	0.267	5.1±1.3	D	[5]	B2110+27	0.298	30	S_d	[2]
B1530+27	0.108	6±2	S_d	[9]	B2111+46	0.135	8.7±0.5	T	[3]
B1604–00	0.805	0.15±0.07	T	[3]	B2122+13	0.454	22	D	[2]
J1649+2533	0.106	25±5	...	[4]	B2154+40	0.191	7.5±2.5	cT	[21]
B1658–37	0.149	14±2	...	[10]	J2253+1516	0.026	49	D	[2]
J1702–4428	0.068	26±3	...	[10]	B2303+30	0.146	5.3±0.5	S_d	[5]
B1700–32	0.073	0.9±0.2	T	[5]	B2310+42	0.52	4.5±0.6	cT	[3]
B1706–16	4.47	31±2	S_t	[11]	B2315+21	0.069	3±0.5	cT	[9]
B1713–40	1.04	80±15	S_t	[12]	B2319+60	1.21	15.2±1.1	cQ	[3]
J1725–4043	0.175	<70	...	[13]	B2327–20	0.206	11.2±1.0	T	[3]
J1727–2739	0.101	68.2±1.1	D	[14]	J2346–0609	0.163	35.6±2.2	D	[5]
J1738–2330	0.218	> 69	...	[13]					

NOTE.—1-Huguenin *et al.* (1970); 2-Redman & Rankin (2009); 3-This paper; 4-Herfindal & Rankin (2009); 5-Basu *et al.* (2017); 6-Basu & Mitra (2019); 7-Kawash *et al.* (2018); 8-Biggs (1992); 9-Weisberg *et al.* (1986); 10-Wang *et al.* (2007); 11-Naidu *et al.* (2018); 12-Kerr *et al.* (2014); 13-Gajjar *et al.* (2012); 14-Wen *et al.* (2016); 15-Lewandowski *et al.* (2004); 16-Basu & Mitra (2018b); 17-Gajjar *et al.* (2017); 18-Rosen *et al.* (2013); 19-Lorimer *et al.* (2002); 20-Basu *et al.* (2019b); 21-Ritchings (1976)

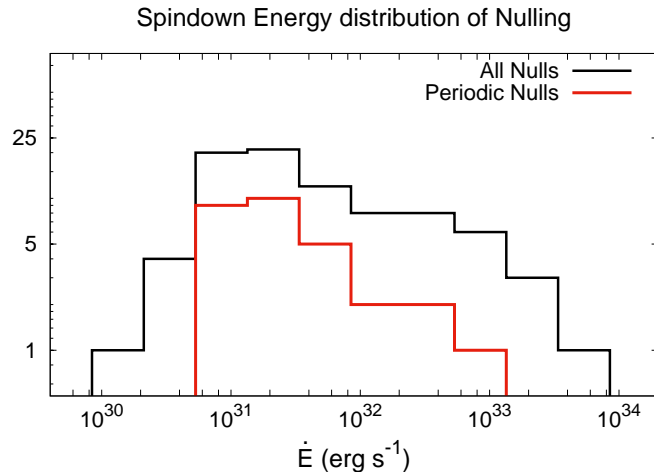


Fig. 6.— The figure shows \dot{E} distribution of pulsars showing the presence of nulling in their single pulse sequences. The black histograms shows the distribution for the entire nulling population, while the red plot corresponds to the subgroup showing periodic nulling.

sources was compiled from the literature as well as newer observations using GMRT. We have carried out detailed nulling and periodic modulation analysis in sixty two pulsars. Our studies found nulling in twenty pulsars and periodic modulations in twenty four cases. We detected periodic nulling in ten pulsars, eight of which were new detections, expanding this population to twenty nine pulsars. We have identified eighteen pulsars to exhibit periodic amplitude modulation, not associated with nulling, which is the first such categorization of this behaviour. Additionally, we have also identified twenty four pulsars with periodic modulation, where detection sensitivities were insufficient to distinguish between the two phenomena.

Most periodic modulations have been considered a form of subpulse drifting in a majority of past studies. We have compared periodic behaviour associated with subpulse drifting and other periodic modulations and found them to exhibit different physical properties. The different periodic modulations on the other hand exhibit similar characteristics, like overlapping periodicities along \dot{E} and longitude stationary behaviour across all profile components, which suggest similar physical mechanisms. We have also found periodic nulling to be a significant subset of the nulling phenomenon in general with no clear distinctions in physical properties.

Acknowledgments

We thank the referee for the comments which helped to improve the paper. DM acknowledges funding from the grant “Indo-French Centre for the Promotion of Advanced Research - CEFIPRA”. We thank the staff of the GMRT who have made these observations possible. The GMRT is run by the National Centre for Radio Astrophysics of the Tata Institute of Fundamental Research.

REFERENCES

- Backer, D.C. 1970a, *Nature*, 228, 692
- Backer, D.C. 1970b, *Nature*, 228, 42
- Backer, D.C. 1970c, *Nature*, 228, 1297
- Backer, D.C. 1973, *ApJ*, 182, 245
- Becker, W. 2009, *Neutron Stars and Pulsars*, *Astrophysics and Space Science Library*, 357, 91
- Basu, R.; Mitra, D.; Melikidze, G.I.; Maciesiak, K.; Skrzypczak, A.; Szary, A. 2016, *ApJ*, 833, 29
- Basu, R.; Mitra, D.; Melikidze, G.I. 2017, *ApJ*, 846, 109
- Basu, R.; Mitra, D. 2018a, *MNRAS*, 475, 5098

- Basu, R.; Mitra, D. 2018b, MNRAS, 476, 1345
- Basu, R.; Mitra, D.; Melikidze, G.I.; Skrzypczak, A. 2019a, MNRAS, 482, 3757
- Basu, R.; Paul, A.; Mitra, D. 2019b, MNRAS, 486, 5216
- Basu, R.; Mitra, D. 2019, MNRAS, 487, 4536
- Biggs, J.D. 1992, ApJ, 394, 574
- Deshpande, A.A.; Rankin, J.M. 2001, ApJ, 322, 438
- Drake, F.D.; Craft, H.D. 1968, Nature, 220, 231
- Goldreich, P.; Julian, W.H. 1969, ApJ, 157, 869
- Gajjar, V.; Joshi, B.C.; Kramer, M. 2012, MNRAS, 424, 1197
- Gajjar, V.; Yuan, J.P.; Yuen, R.; Wen, Z.G.; Liu, Z.Y.; Wang, N. 2017, ApJ, 850, 173
- Force, M.M.; Rankin, J.M. 2010, MNRAS, 406, 237
- Gil, J.; Sendyk, M. 2000, ApJ, 541, 351
- Gil, J.; Melikidze, G.I.; Geppert, U. 2003, A&A, 407, 315
- Herfindal, J.L.; Rankin, J.M. 2007, MNRAS, 380, 430
- Herfindal, J.L.; Rankin, J.M. 2009, MNRAS, 393, 1391
- Hermesen, W.; Kuiper, L.; Hessels, J. W. T.; *et al.* 2017, MNRAS, 466, 1688
- Huguenin, G.R.; Taylor, J.H.; Troland, T.H. 1970, ApJ, 162, 727
- Kawash A.M.; *et al.* 2018, ApJ, 857, 131
- Kerr, M.; Hobbs, G.; Shannon, R.M.; Kiczynski, M.; Hollow, R.; Johnston, S. 2014, MNRAS, 445, 320
- Latham, C.; Mitra, D.; Rankin, J. 2012, MNRAS, 427, 180
- Lewandowski, W.; Wolszczan, A.; Feiler, G.; Konacki, M.; Soltysinski, T. 2004, ApJ, 600, 905
- Lorimer, D.R.; Camilo, F.; Xilouris, K.M. 2002, AJ, 123, 1750
- Mitra, D.; Rankin, J.M. 2011, ApJ, 727, 92
- Mitra, D.; Arjunwadkar, M.; Rankin, J. 2015, ApJ, 806, 236
- Mitra, D.; Basu, R.; Maciesiak, K.; Skrzypczak, A.; Melikidze, G.I.; Szary, A.; Krzeszowski, K. 2016, ApJ, 833, 28
- Mitra, D.; Rankin, J. 2017, ApJ, 468, 4601
- Naidu, A.; Joshi, B.C.; Manoharan, P.K.; Krishnakumar, M.A. 2018, MNRAS, 475, 2375
- Rankin, J.M. 1986, ApJ, 301, 901
- Rankin, J.M. 1990, ApJ, 352, 247
- Rankin, J.M. 1993, ApJ, 405, 285
- Rankin, J.M.; Rodriguez, C.; Wright, G.A.E. 2006, MNRAS, 370, 673
- Rankin, J.M.; Wright, G.A.E. 2008, MNRAS, 385, 1923
- Redman, S.L.; Rankin, J.M. 2009, MNRAS, 395, 1529
- Ritchings, R.T. 1976, ApJ, 176, 249
- Rosen, R.; *et al.* 2013, ApJ, 768, 85
- Ruderman, M.A.; Sutherland, P.G. 1975, ApJ, 196, 51
- Szary, A.; 2013, PhD thesis, Univ. of Zielona Góra, arXiv:1304.4203
- Szary, A.; Melikidze, G.I.; Gil, J. 2015, MNRAS, 447, 2295
- Wang N.; Manchester R. N.; Johnston S. 2007, MNRAS, 377, 1383
- Wahl, H.M.; Orfeo, D.J.; Rankin, J.M.; Weisberg, J.M. 2016, MNRAS, 461, 3740
- Weisberg, J.M.; Armstrong, B.K.; Backus, P.R.; Cordes, J.M.; Boriakoff, V.; Ferguson, D.C. 1986, AJ, 92, 621
- Weltevrede, P.; Edwards, R. T.; Stappers, B. W. 2006, A&A, 445, 243
- Weltevrede, P.; Edwards, R. T.; Stappers, B. W. 2007, A&A, 469, 607
- Wen, Z.G.; Wang, N.; Yuan, J.P.; Yan, W.M.; Manchester, R.N.; Yuen, R.; Gajjar, V. 2016, A&A, 592, 127

Yan, W.M.; Manchester, R.N.; Wang, N.; Yuan, J.P.;
Wen, Z.G.; Lee, K.J. 2019, MNRAS, 485, 3241

A. Pulse energy and off-pulse distributions for Nulling

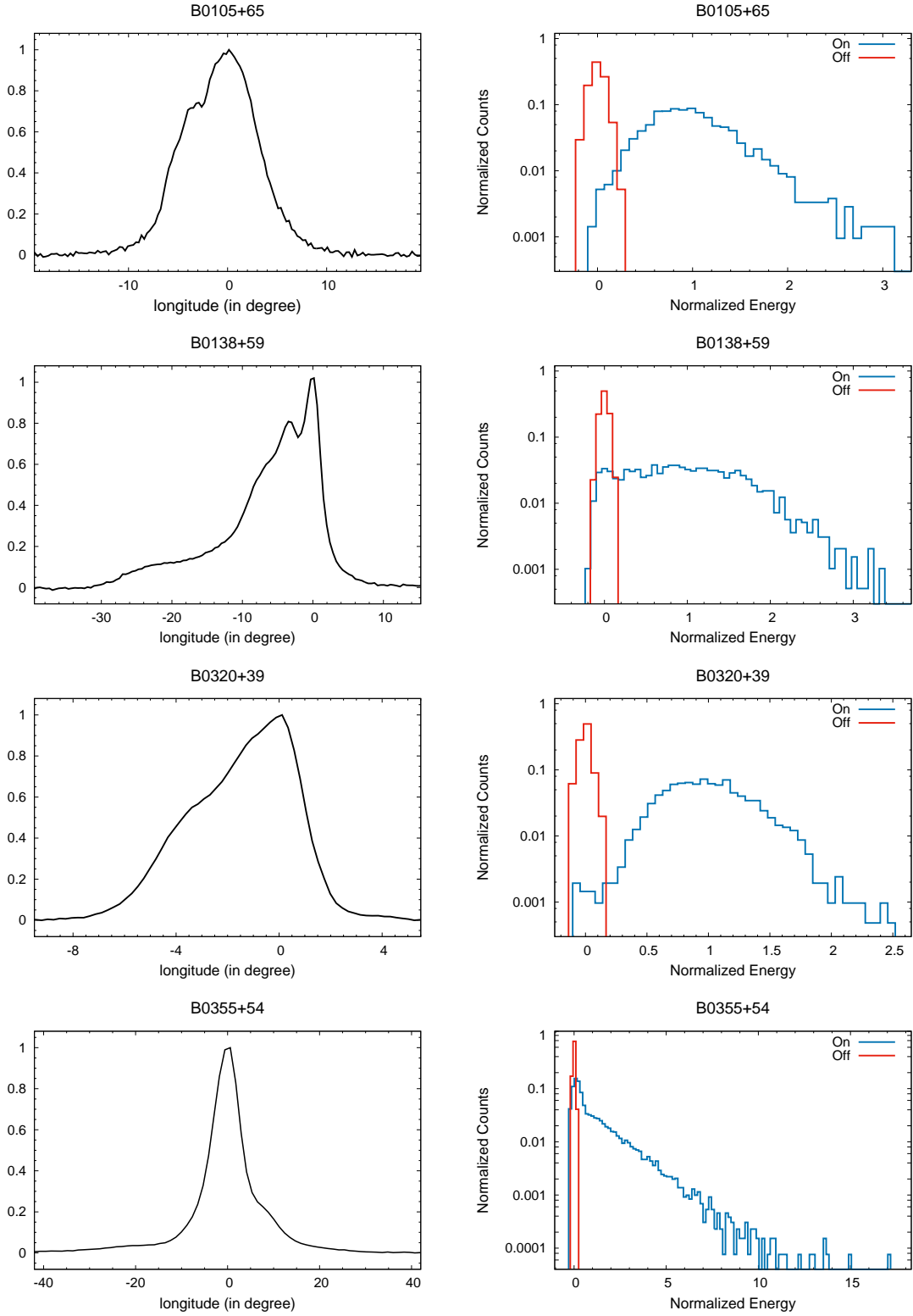


Fig. 7.— The pulsar profile and On and Off-pulse energy distributions of the single pulse emission.

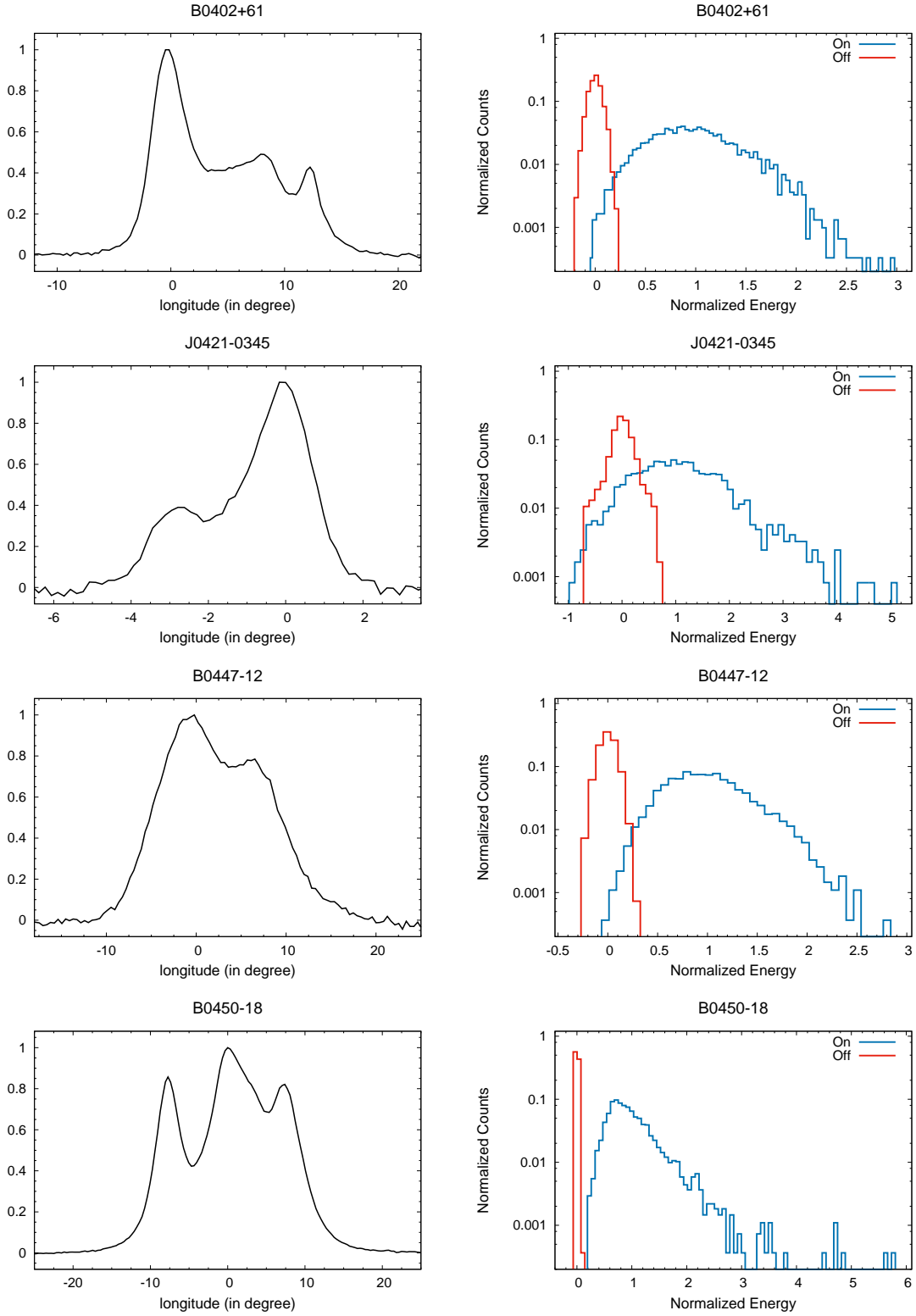


Fig. 8.— The pulsar profile and On and Off-pulse energy distributions of the single pulse emission.

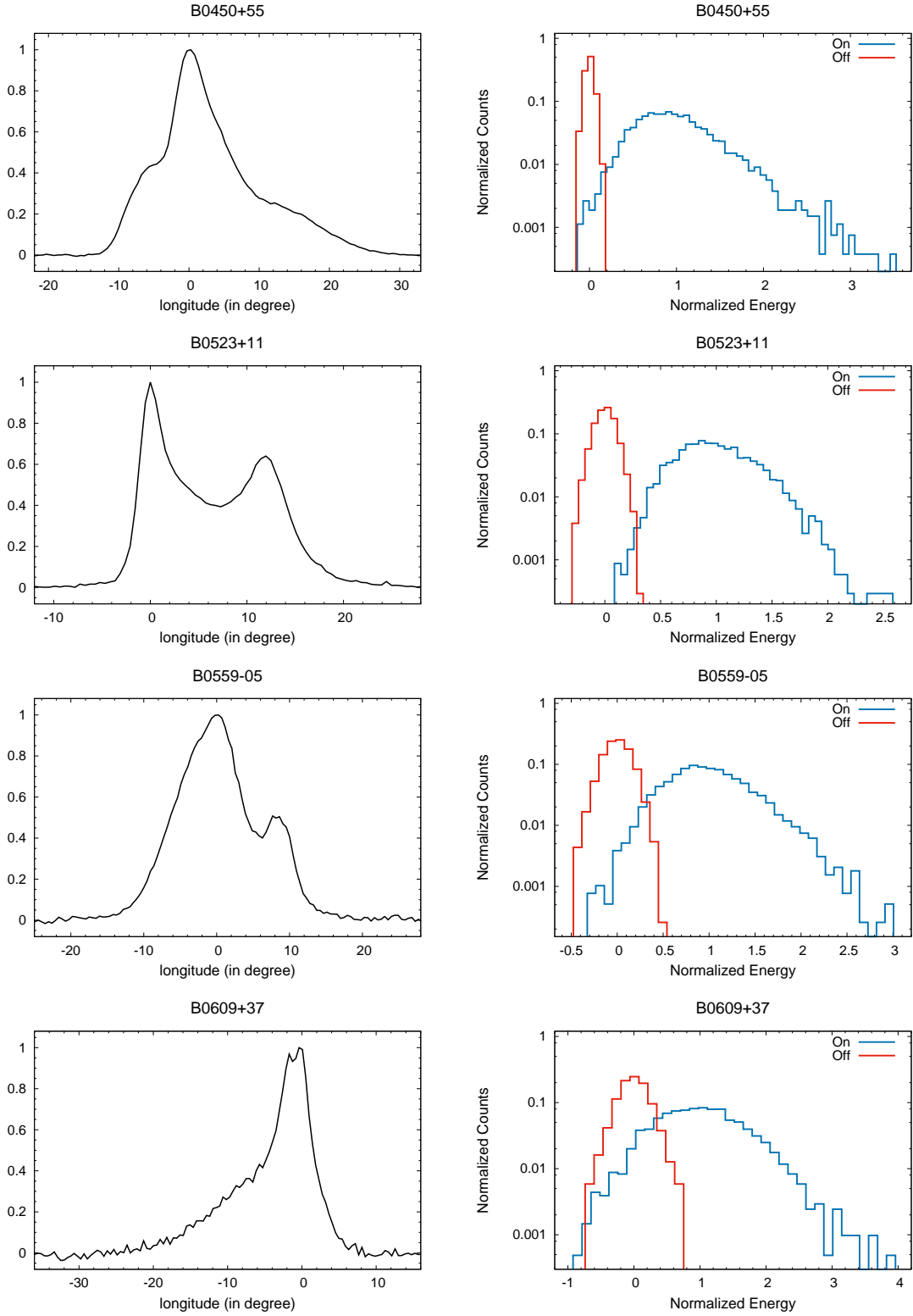


Fig. 9.— The pulsar profile and On and Off-pulse energy distributions of the single pulse emission.

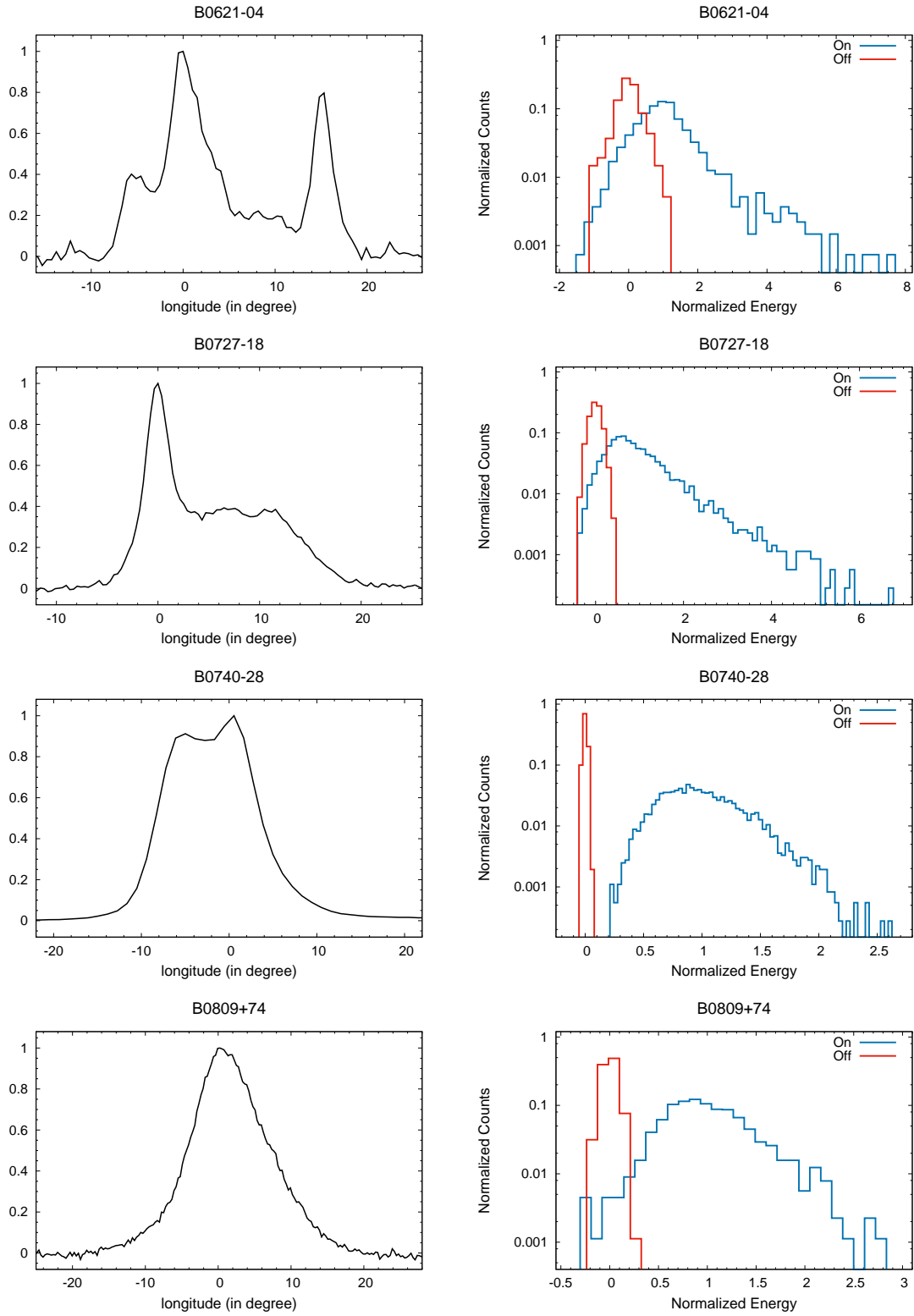


Fig. 10.— The pulsar profile and On and Off-pulse energy distributions of the single pulse emission.

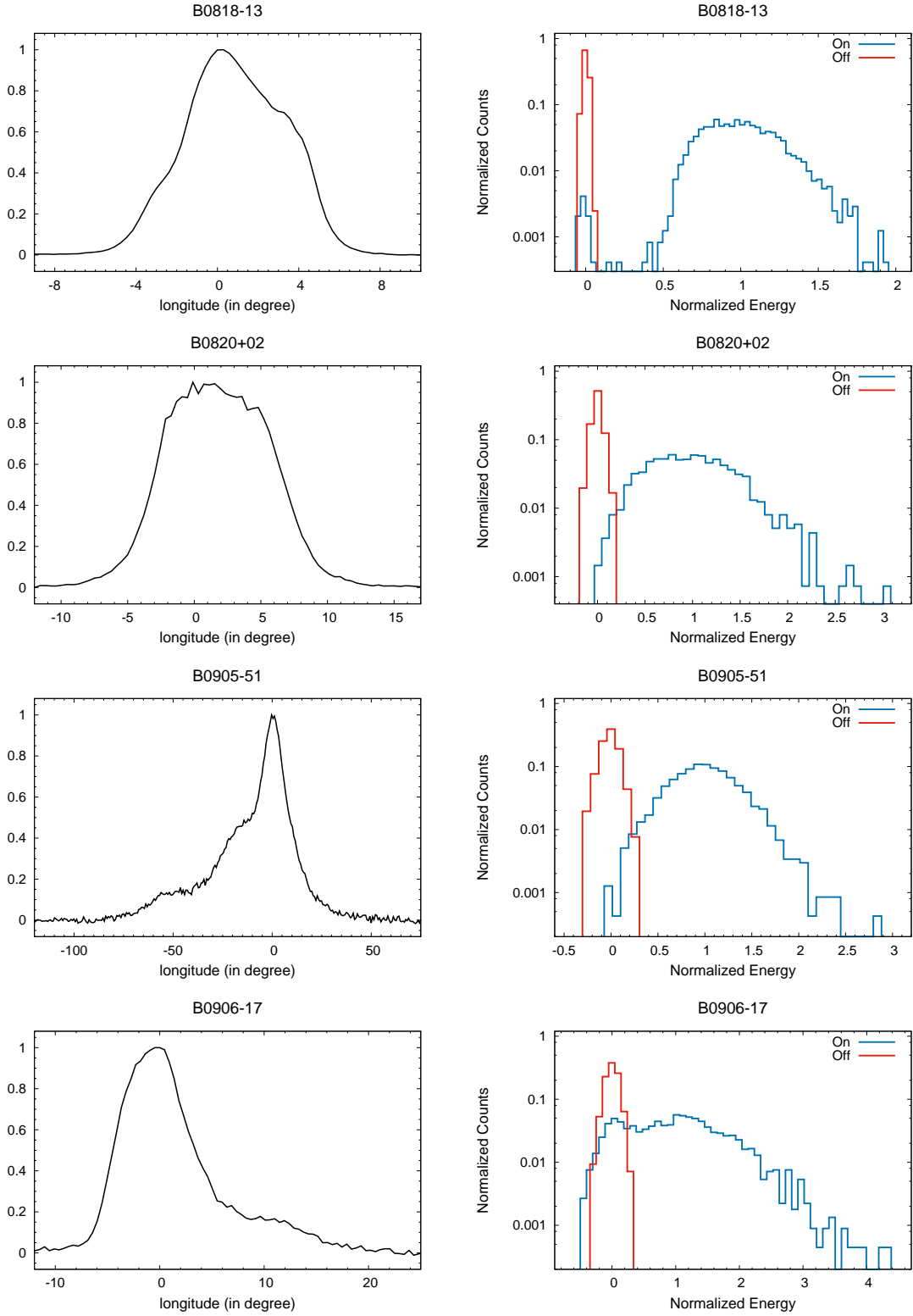


Fig. 11.— The pulsar profile and On and Off-pulse energy distributions of the single pulse emission.

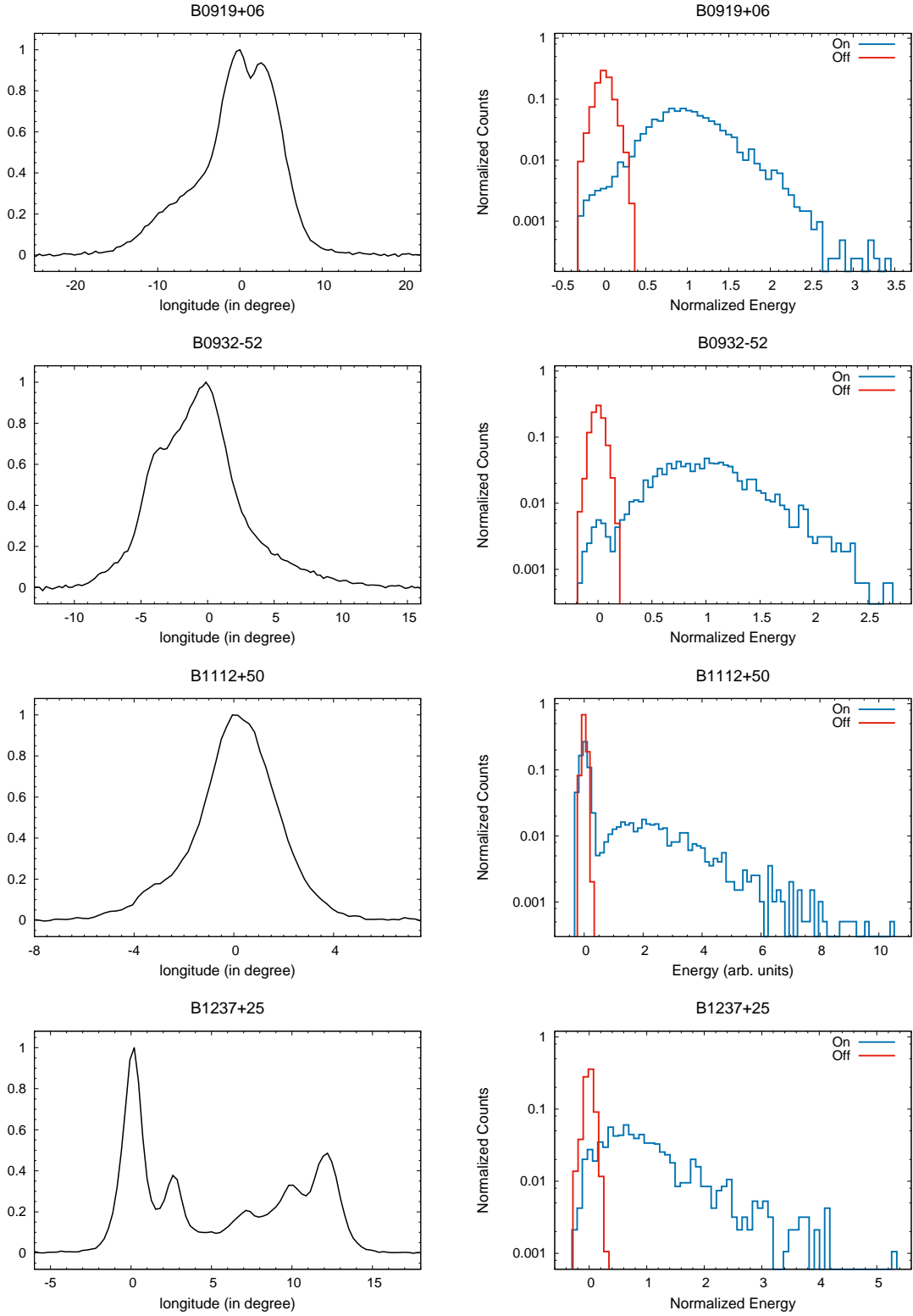


Fig. 12.— The pulsar profile and On and Off-pulse energy distributions of the single pulse emission.

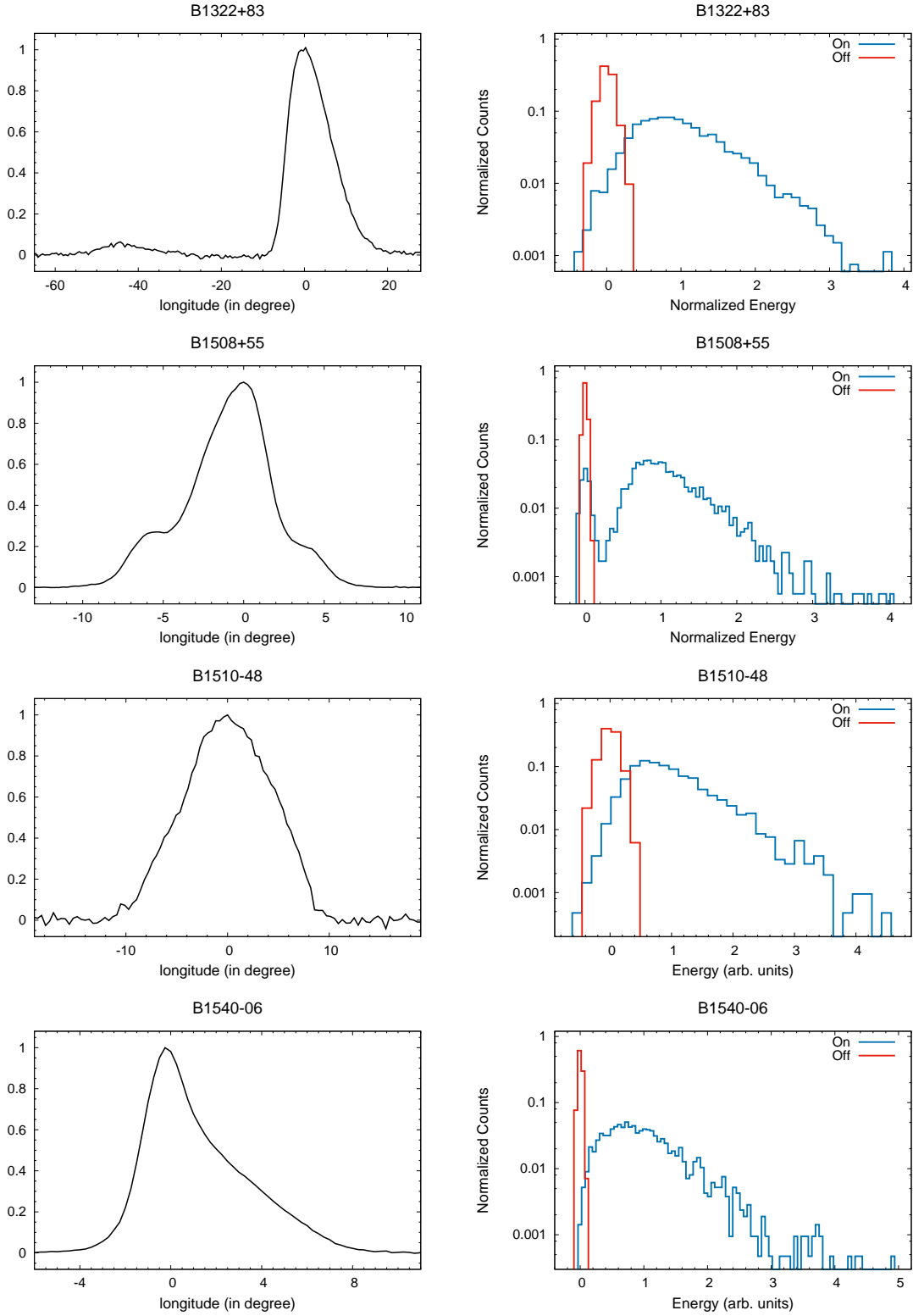


Fig. 13.— The pulsar profile and On and Off-pulse energy distributions of the single pulse emission.

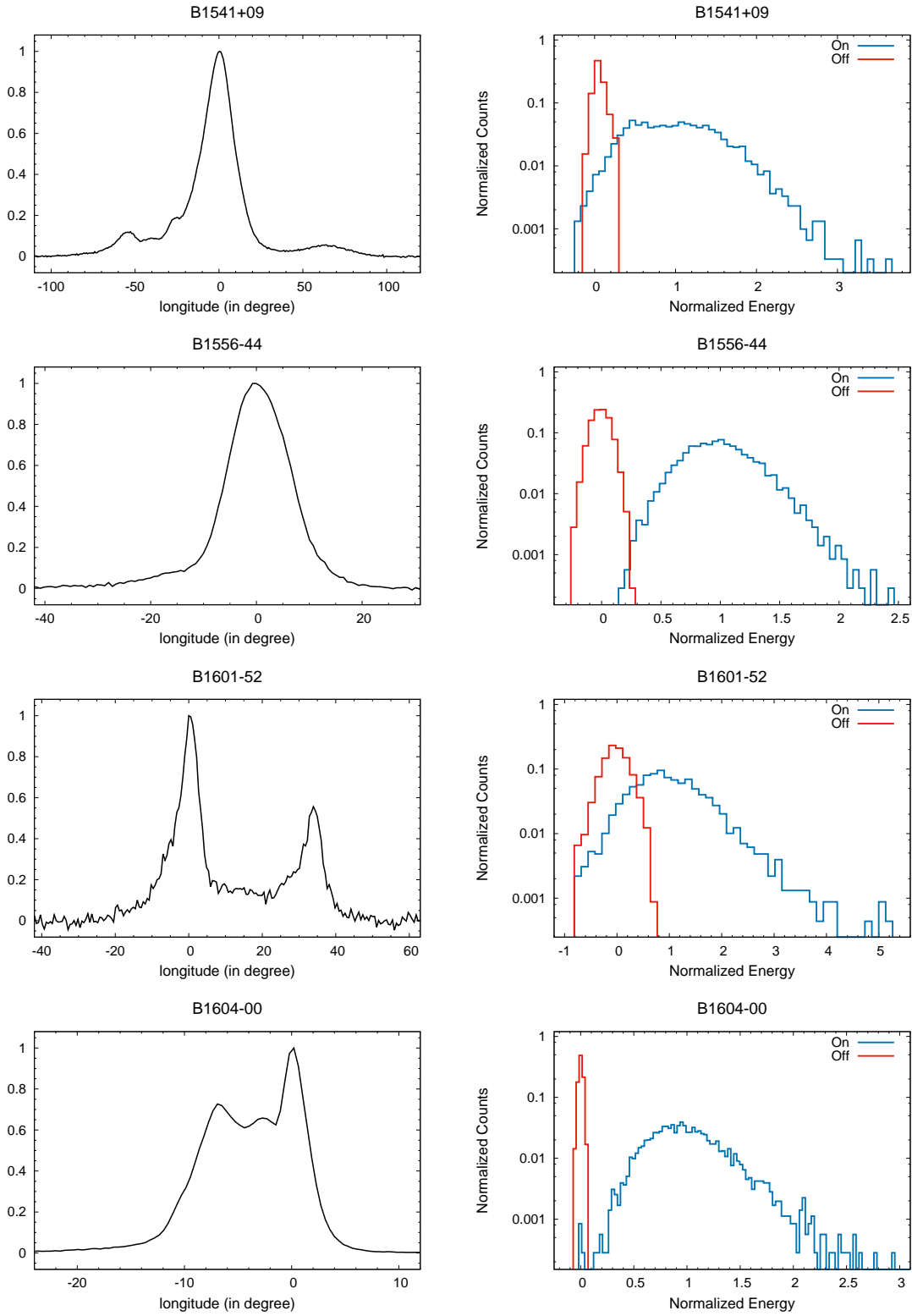


Fig. 14.— The pulsar profile and On and Off-pulse energy distributions of the single pulse emission.

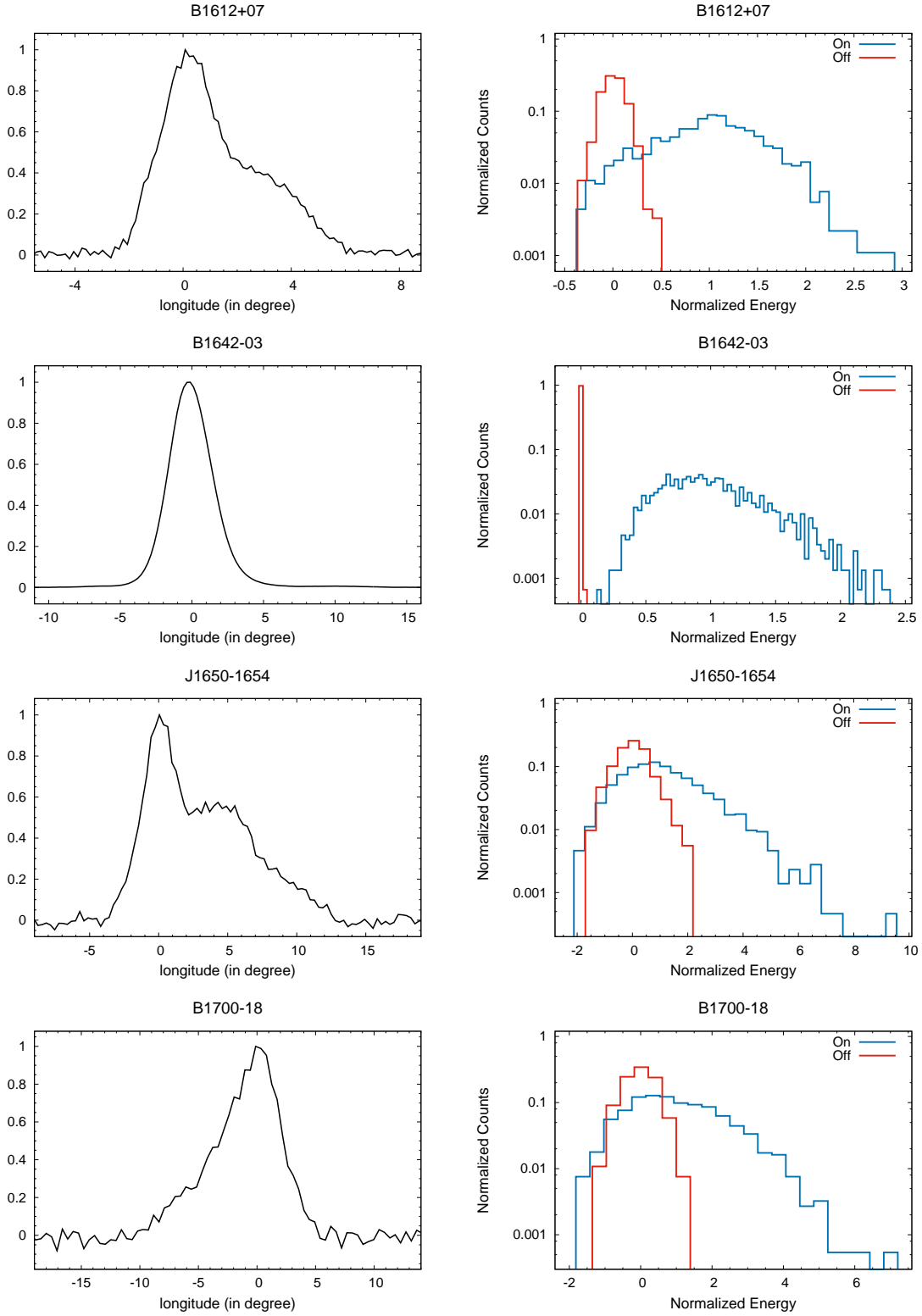


Fig. 15.— The pulsar profile On and Off-pulse energy distributions of the single pulse emission.

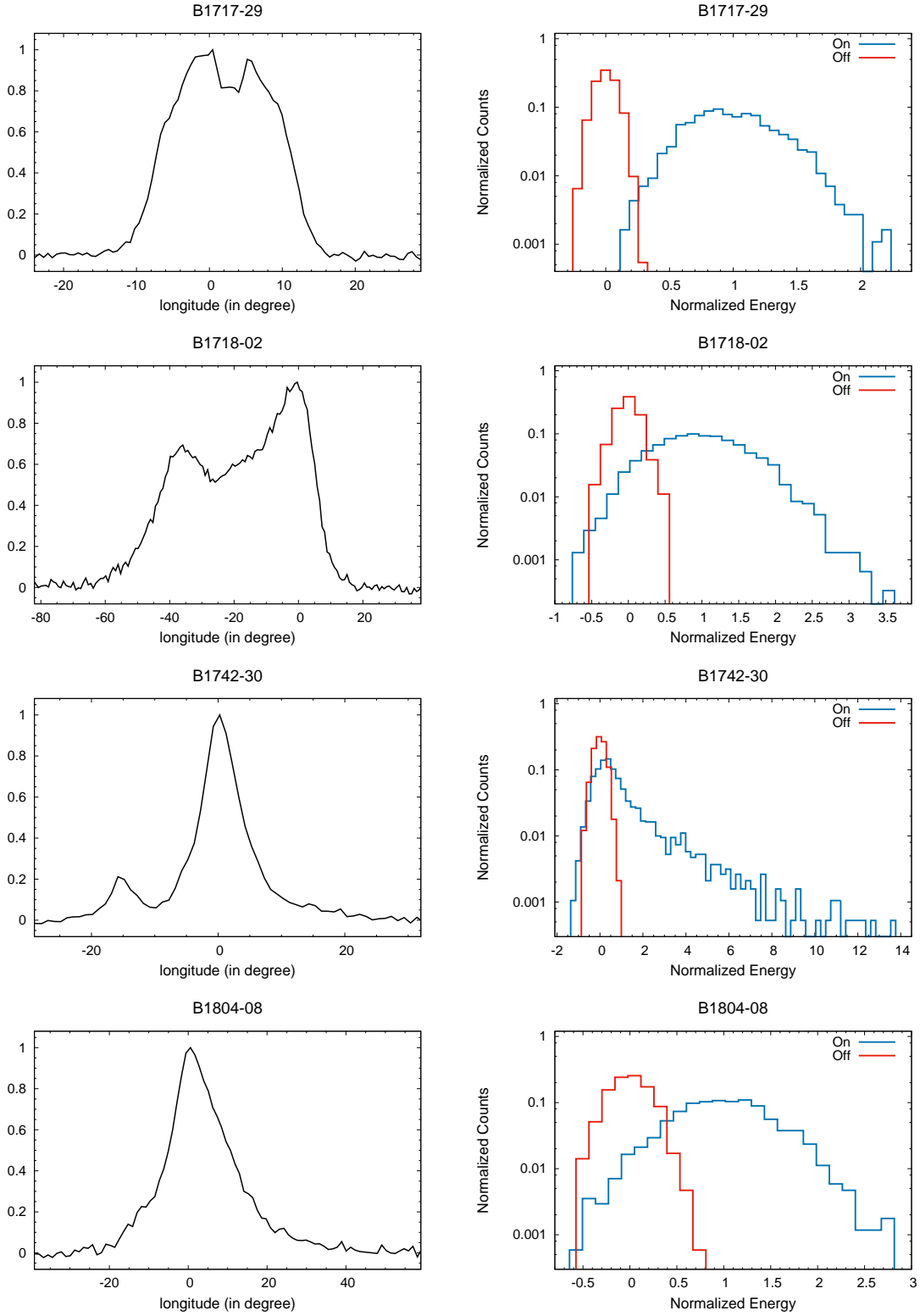


Fig. 16.— The pulsar profile On and Off-pulse energy distributions of the single pulse emission.

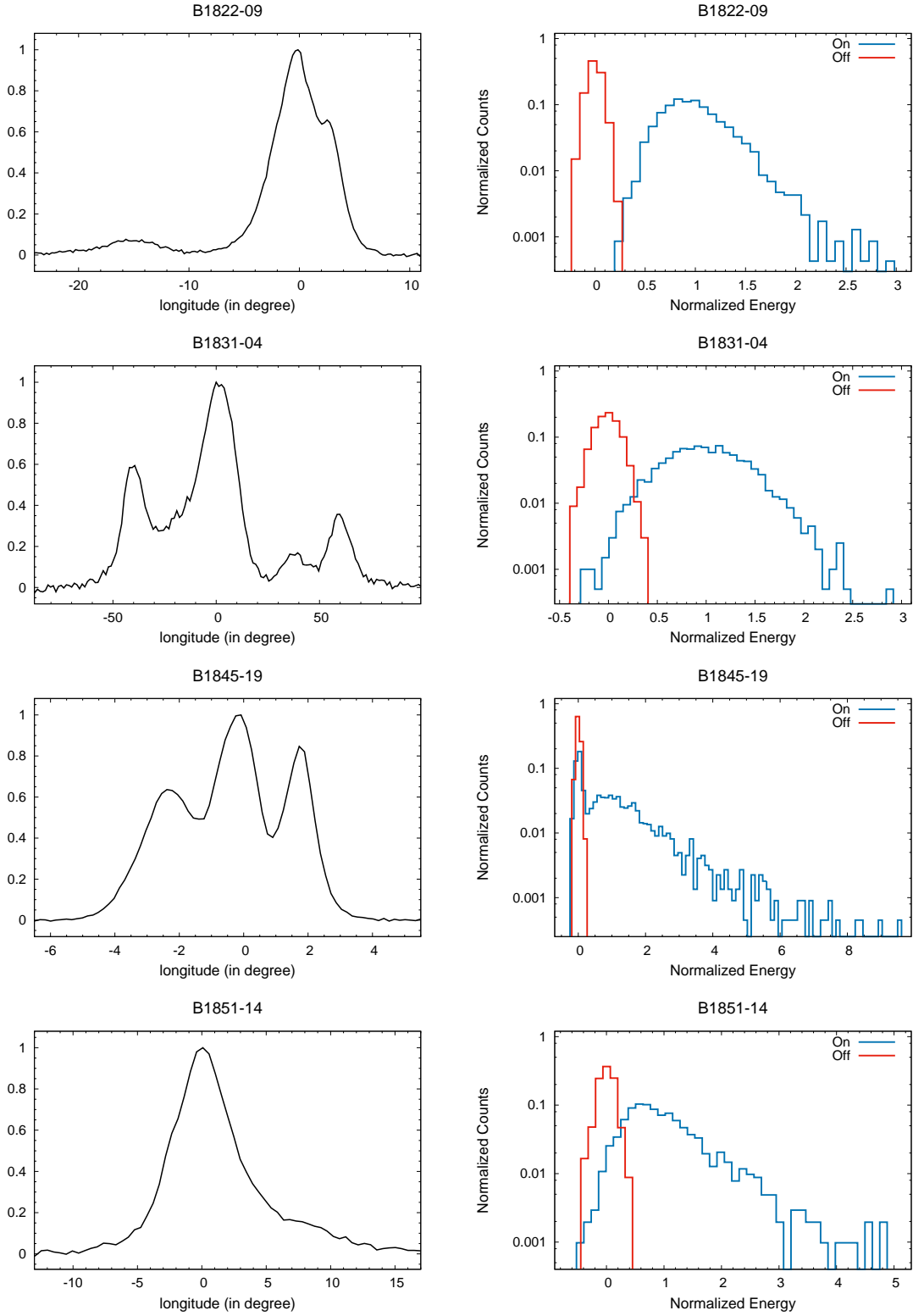


Fig. 17.— The pulsar profile On and Off-pulse energy distributions of the single pulse emission.

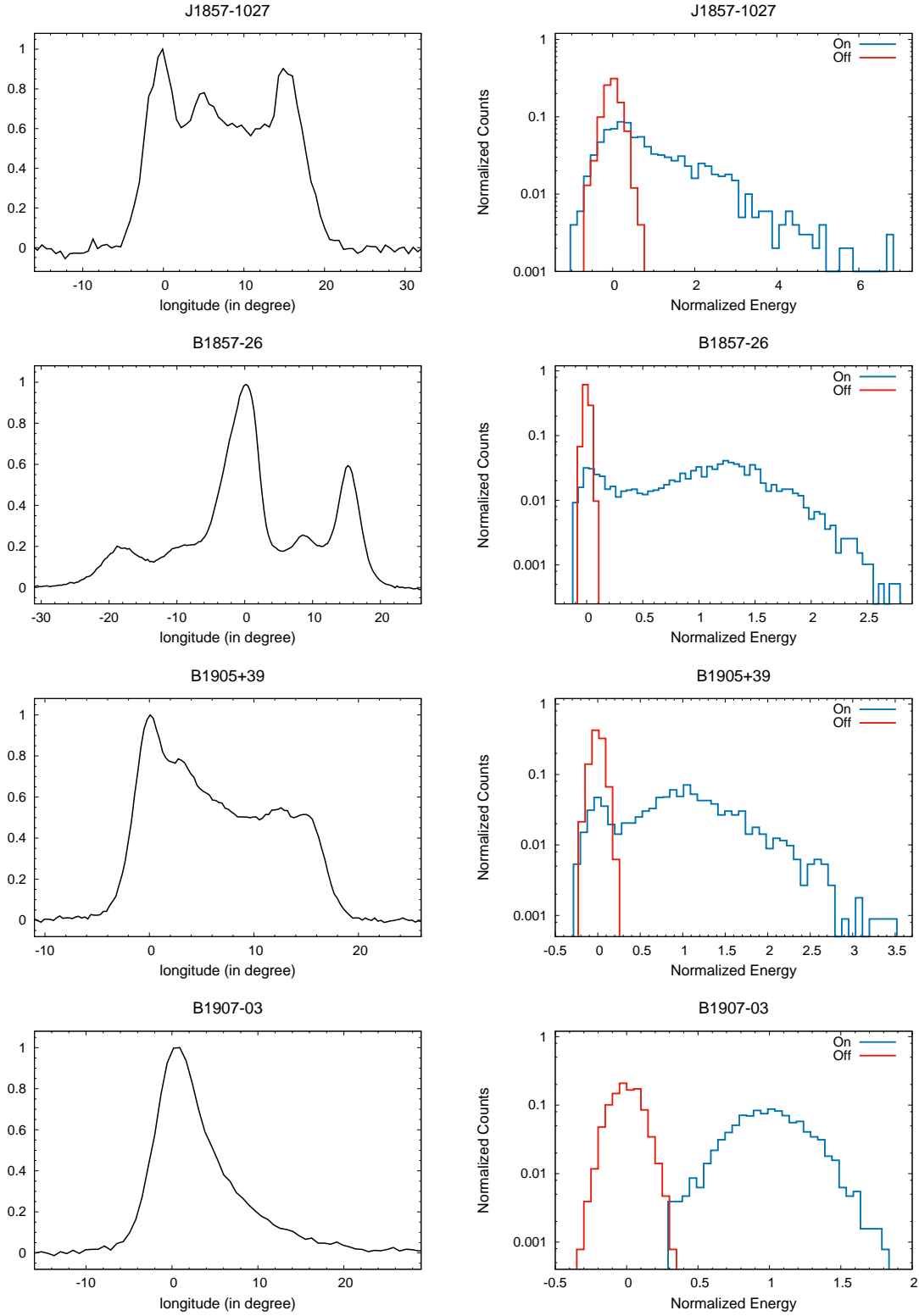


Fig. 18.— The pulsar profile On and Off-pulse energy distributions of the single pulse emission.

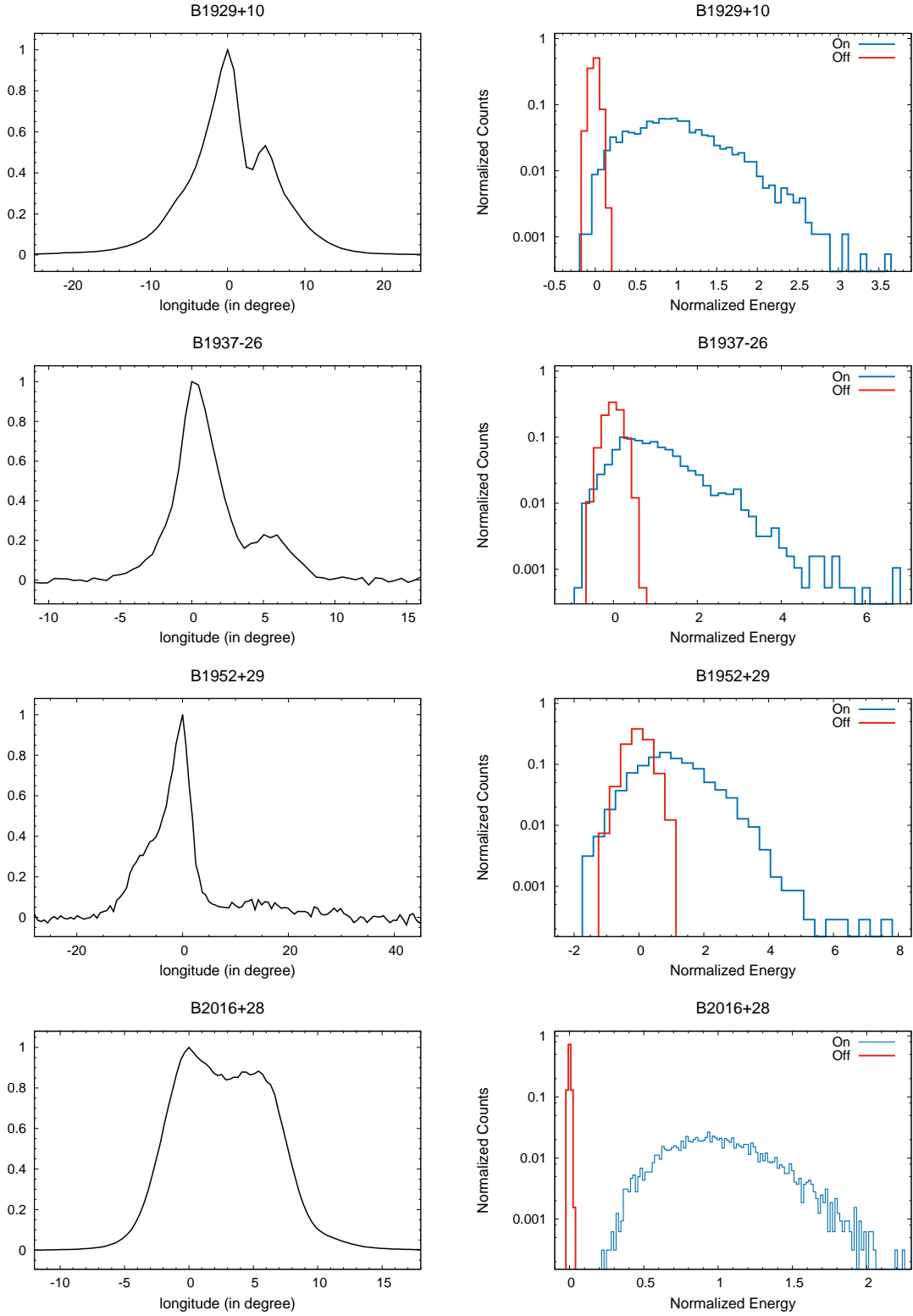


Fig. 19.— The pulsar profile On and Off-pulse energy distributions of the single pulse emission.

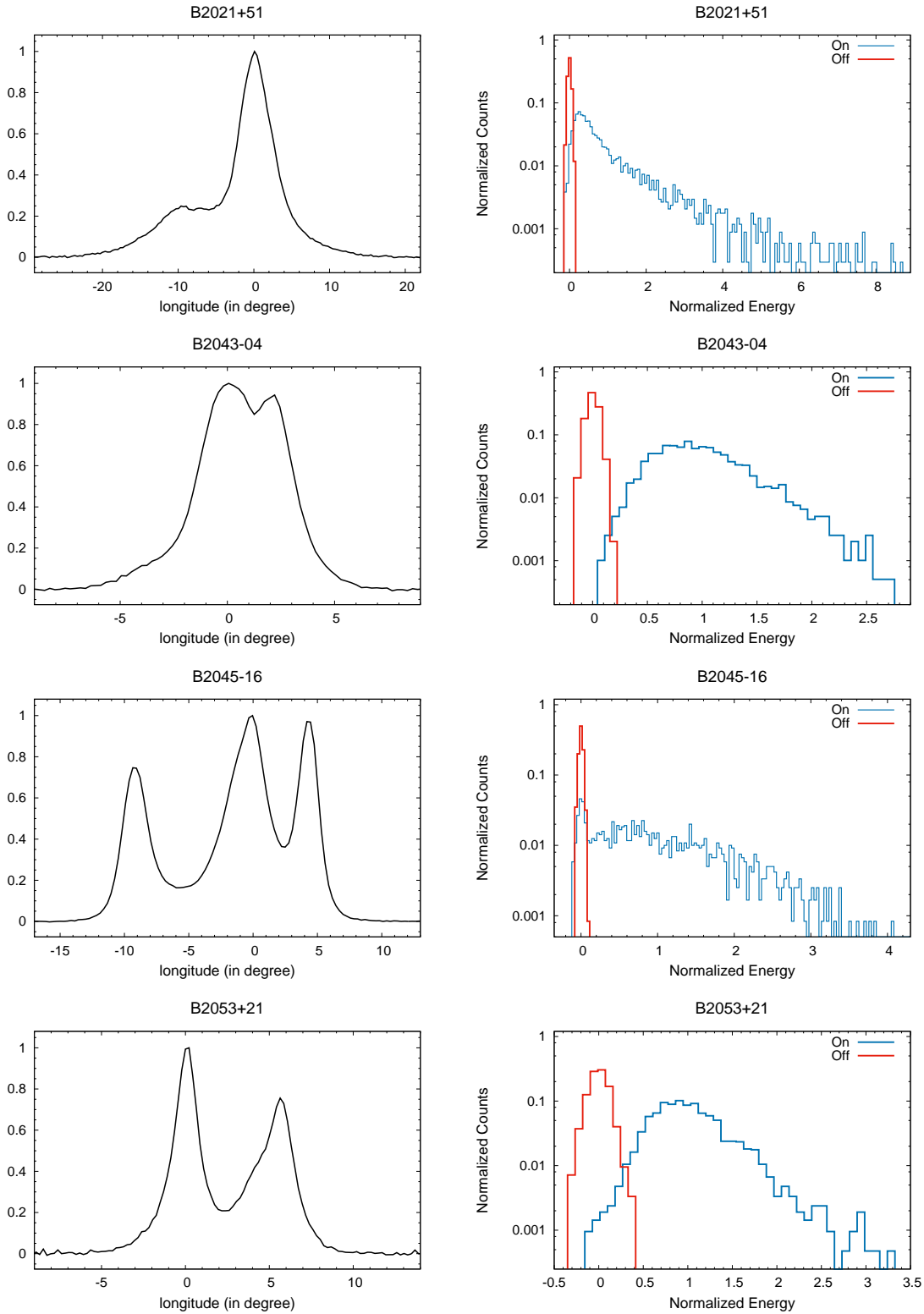


Fig. 20.— The pulsar profile On and Off-pulse energy distributions of the single pulse emission.

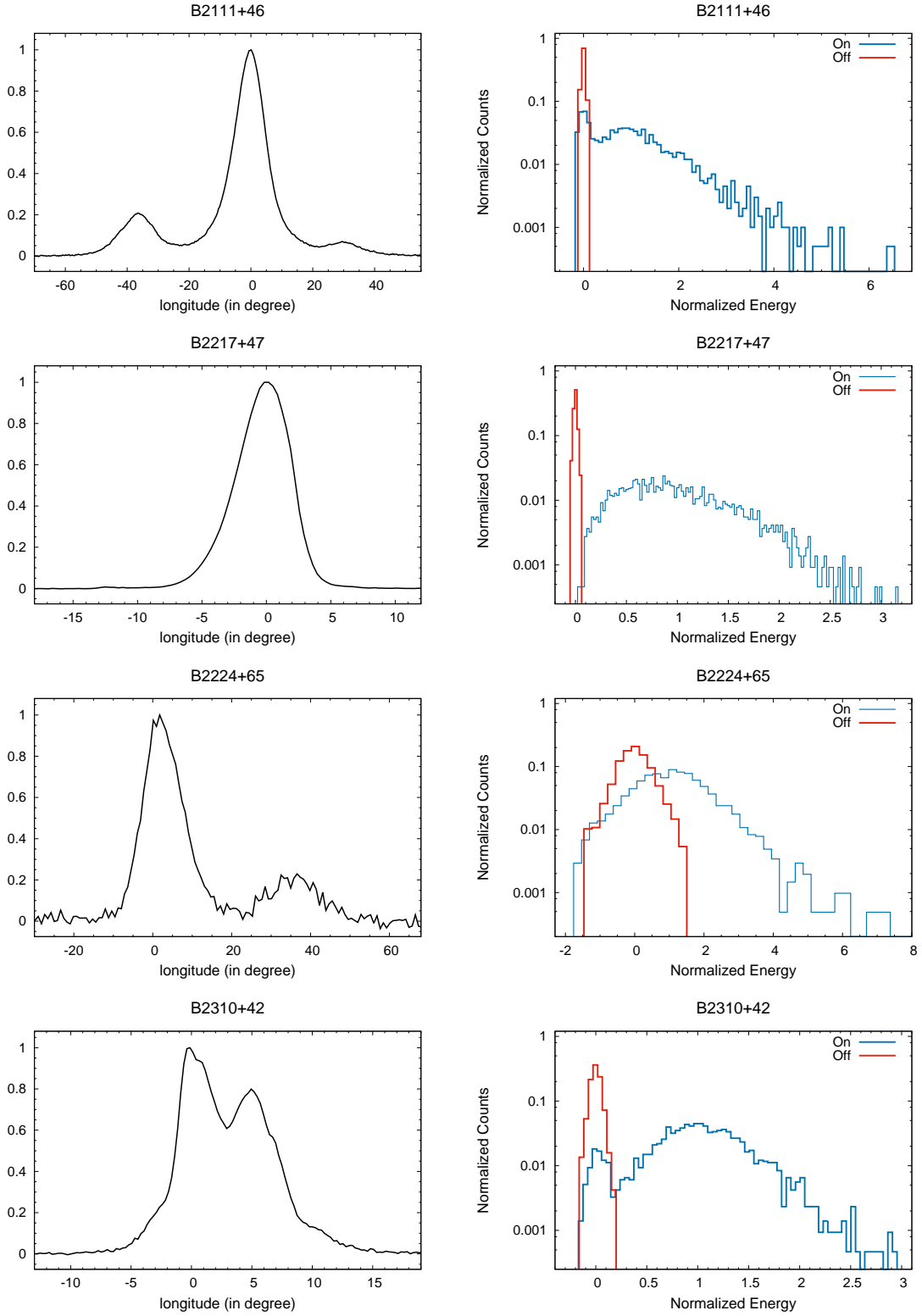


Fig. 21.— The pulsar profile On and Off-pulse energy distributions of the single pulse emission.

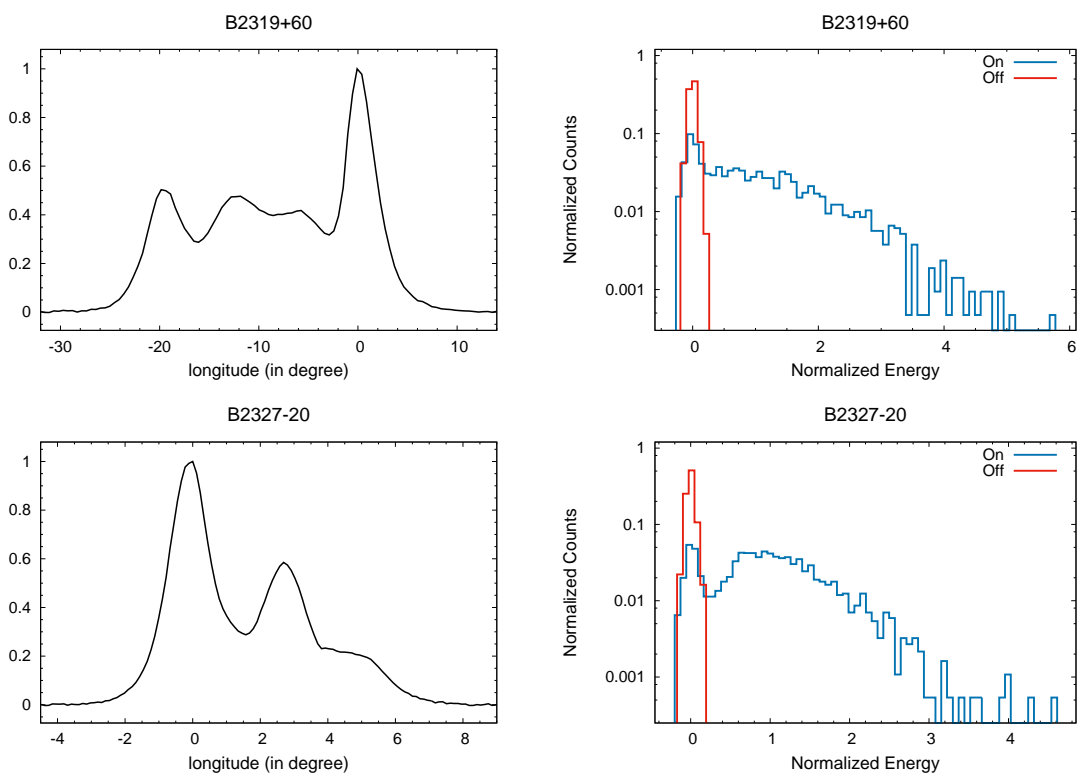


Fig. 22.— The pulsar profile On and Off-pulse energy distributions of the single pulse emission.

B. Null length and Burst length hisograms

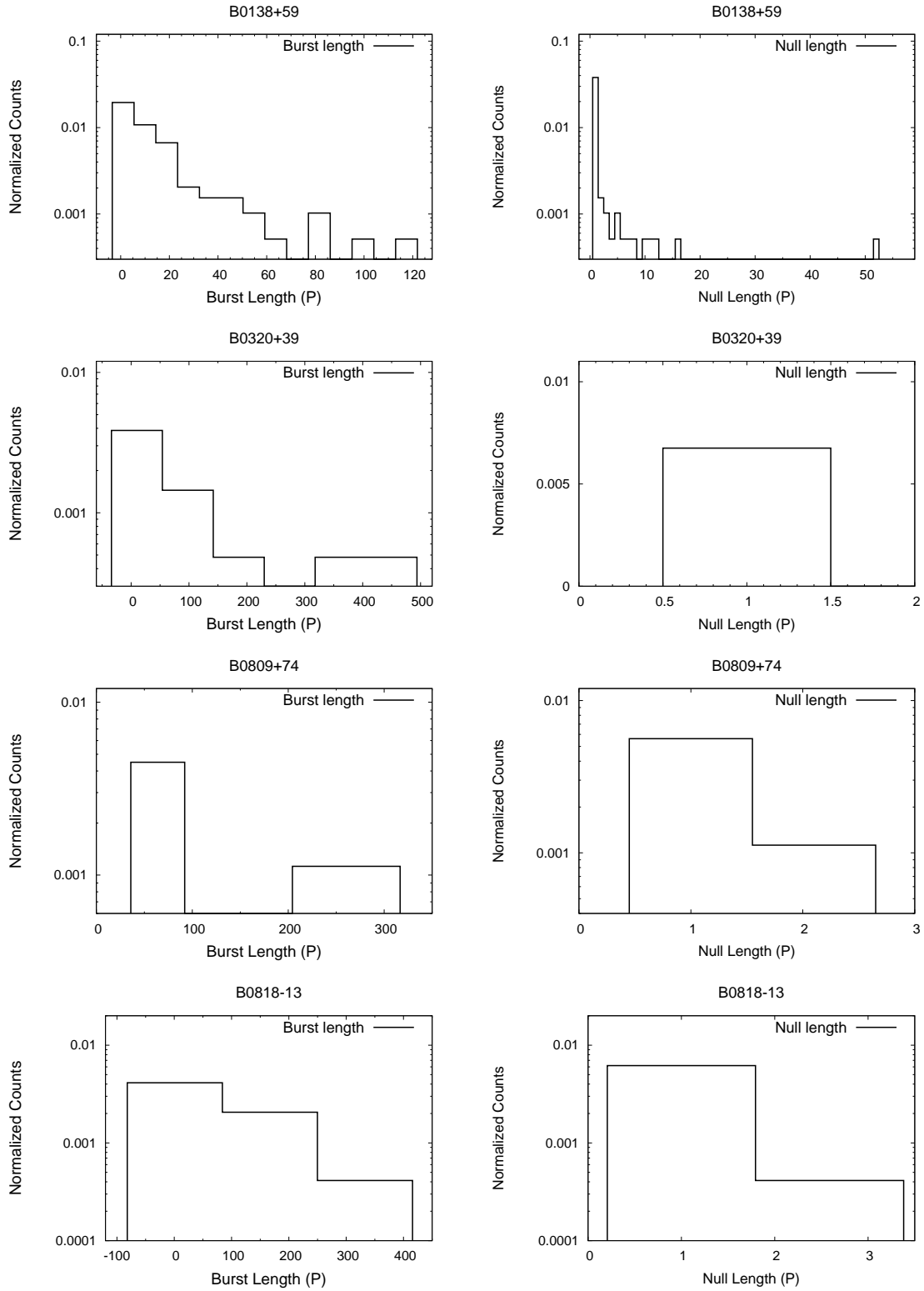


Fig. 23.— The Burst length (left panel) and Null length (right panel) distributions.

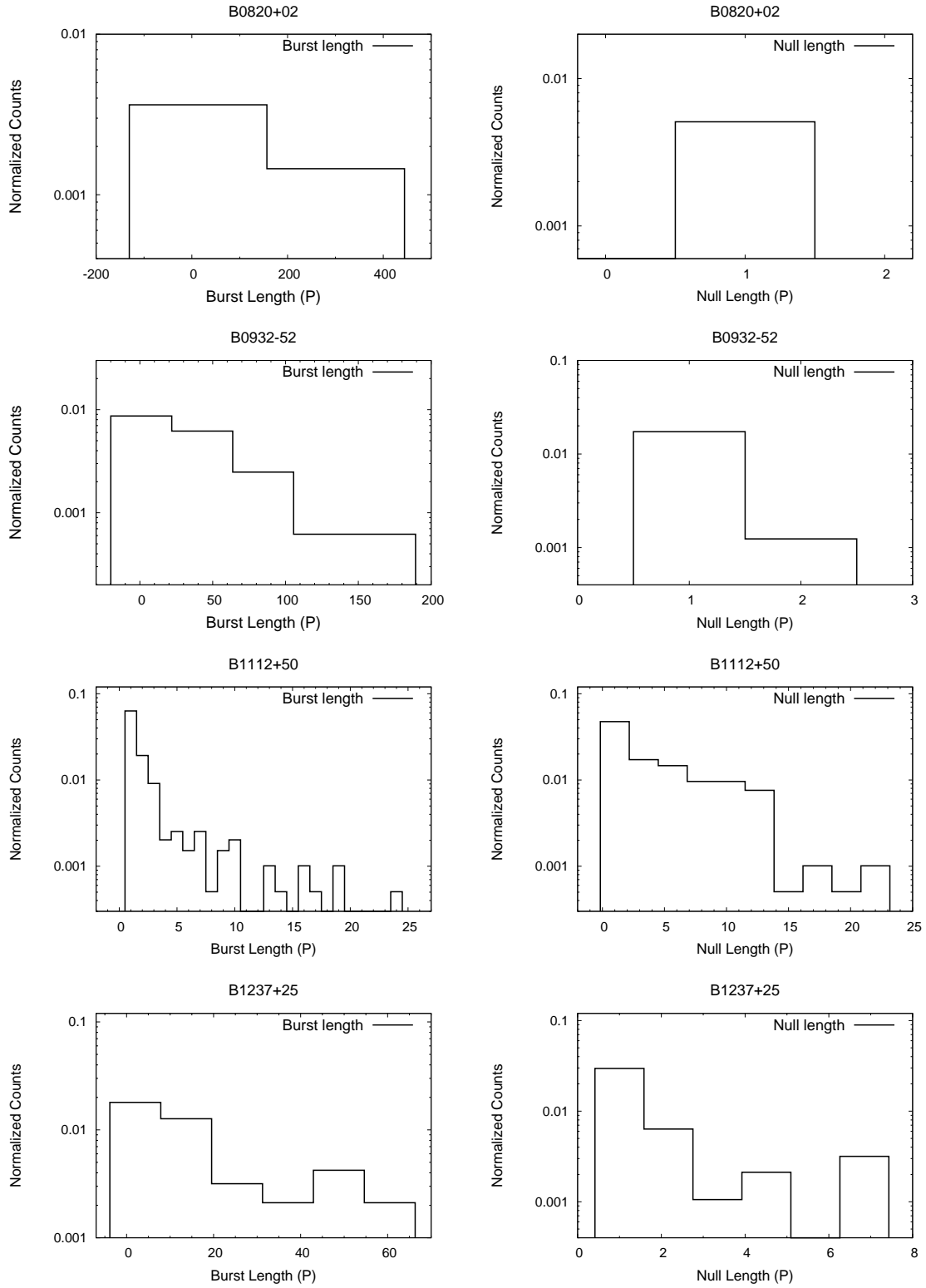


Fig. 24.— The Burst length (left panel) and Null length (right panel) distributions.

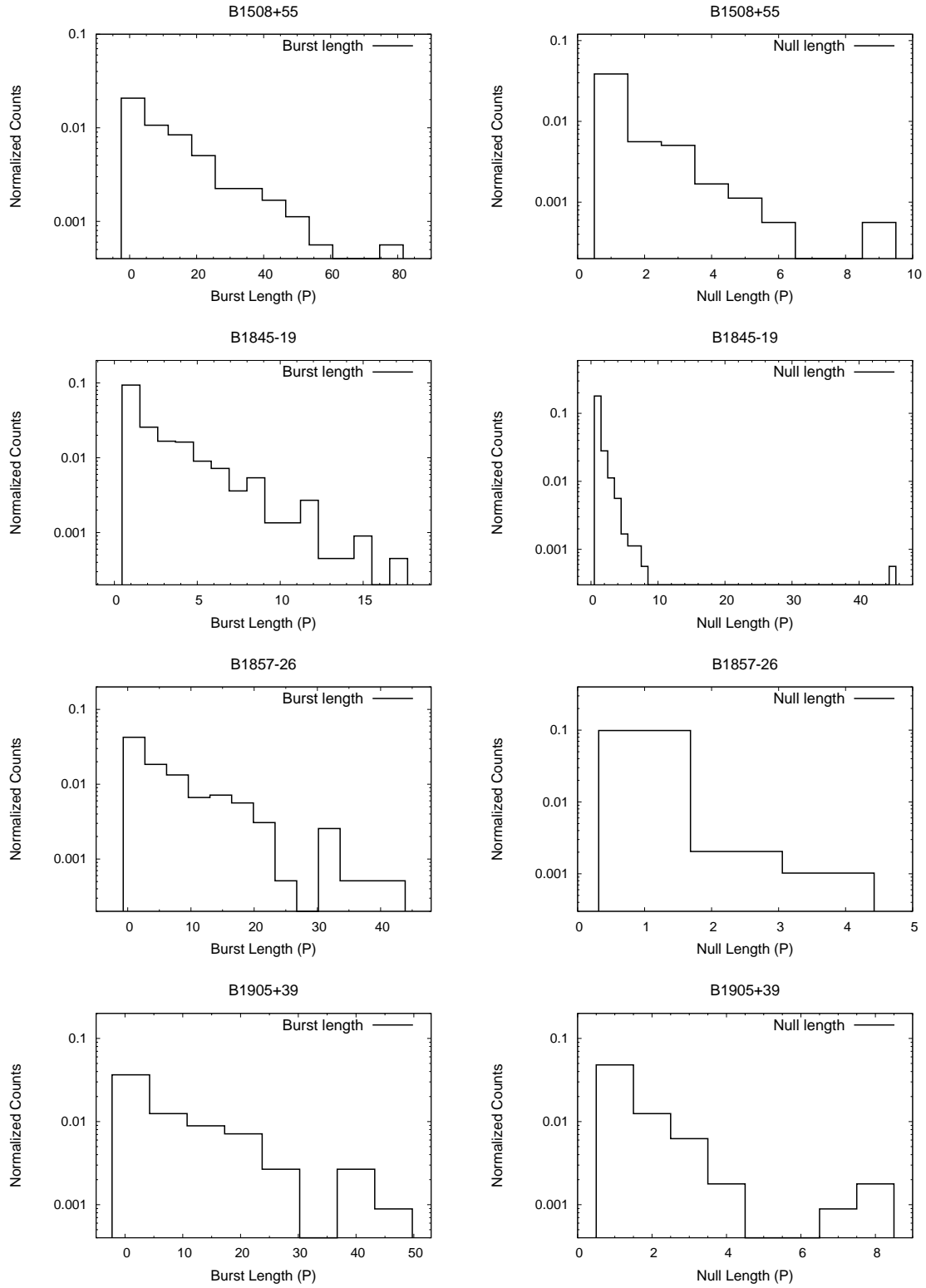


Fig. 25.— The Burst length (left panel) and Null length (right panel) distributions.

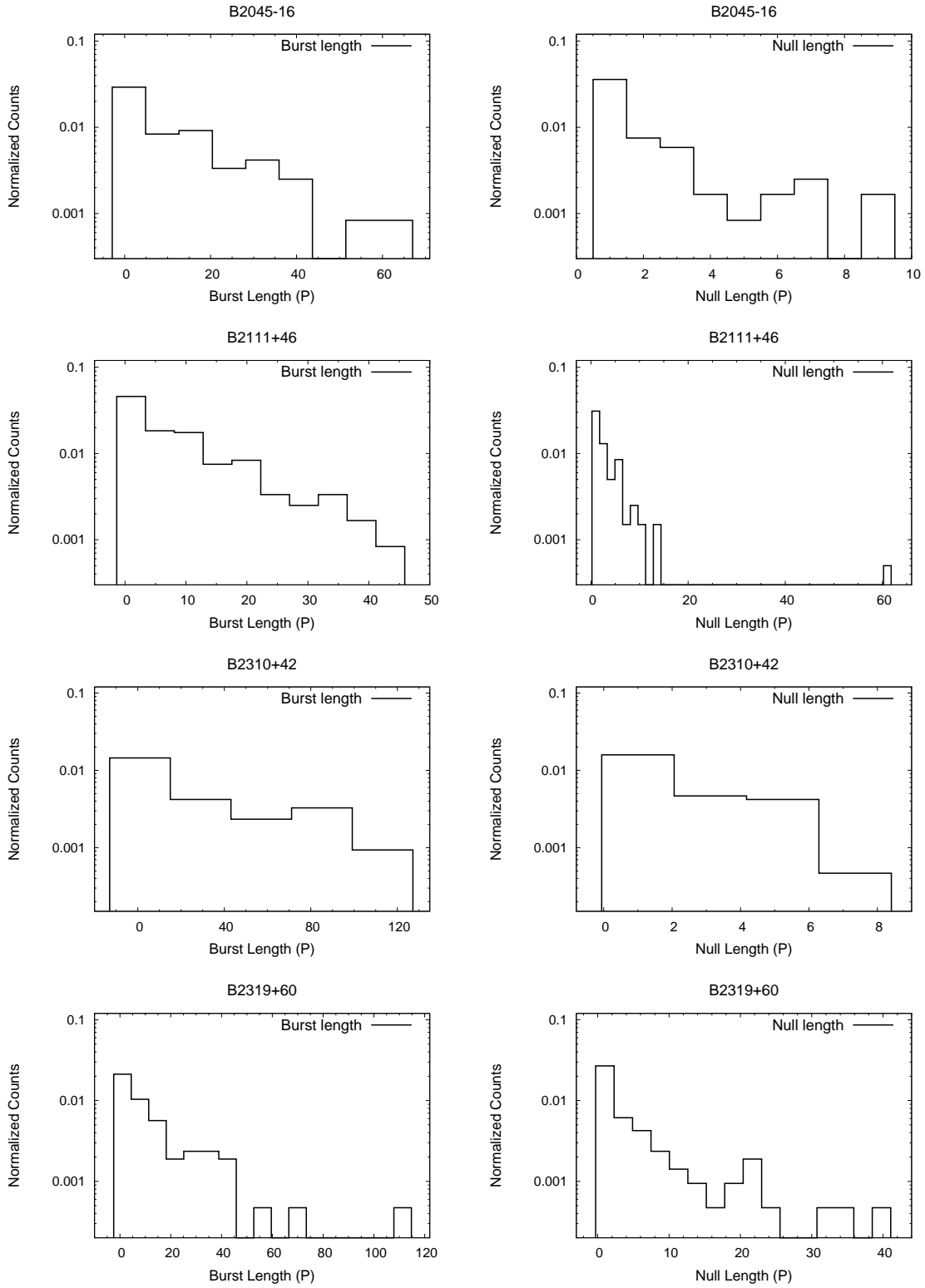


Fig. 26.— The Burst length (left panel) and Null length (right panel) distributions.

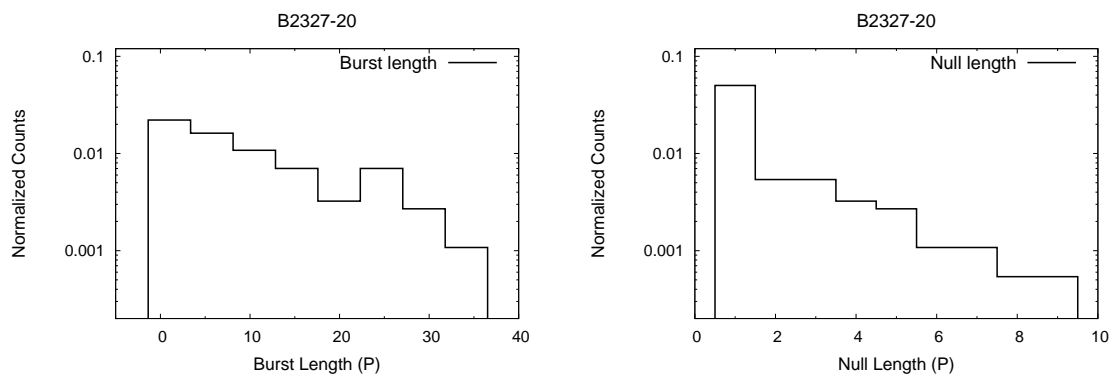


Fig. 27.— The Burst length (left panel) and Null length (right panel) distributions.

C. Time evolution of fluctuation spectra and Nulling FFT

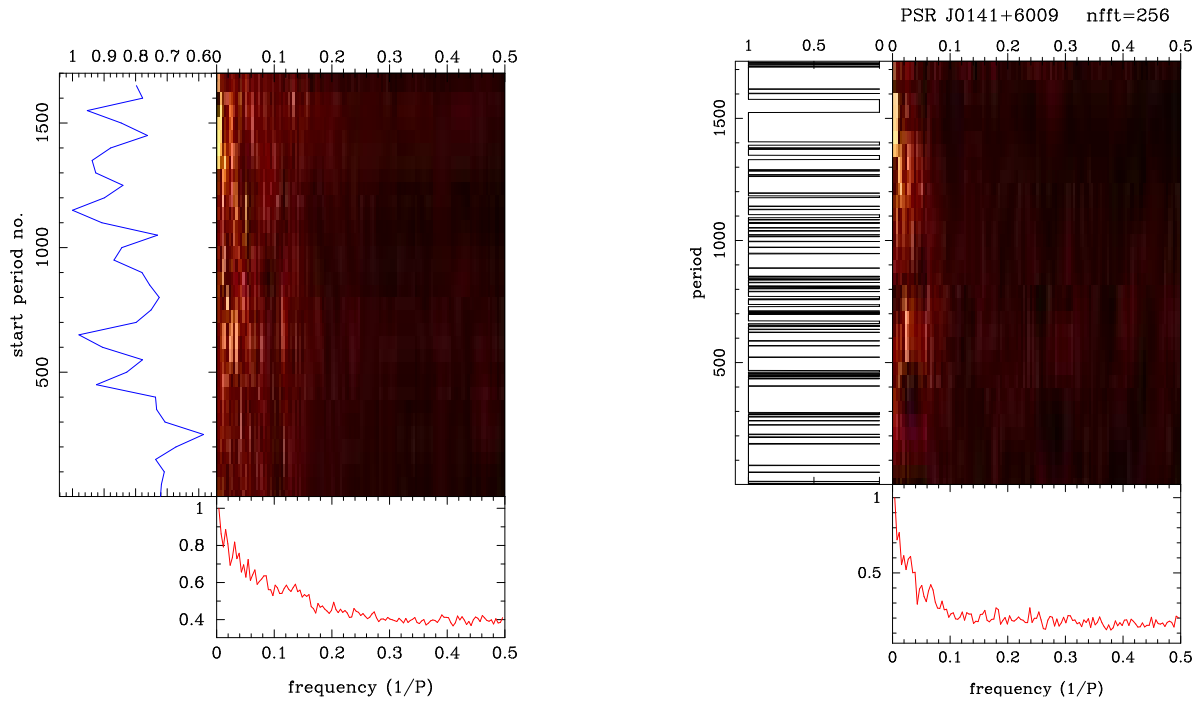


Fig. 28.— PSR B0138+59 : The time evolution of the LRFS (left panel) and the Null-Burst time series FFT (right panel).

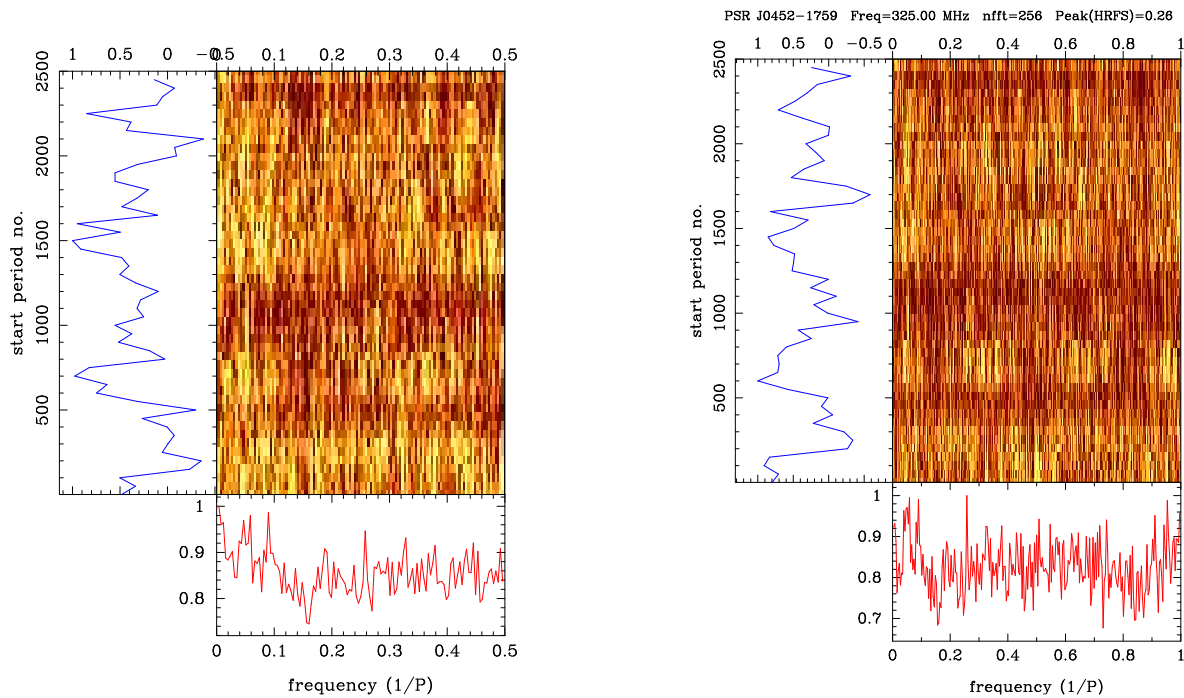


Fig. 29.— PSR B0447-12 : The time evolution of the LRFS (left panel) and the HRFS (right panel).

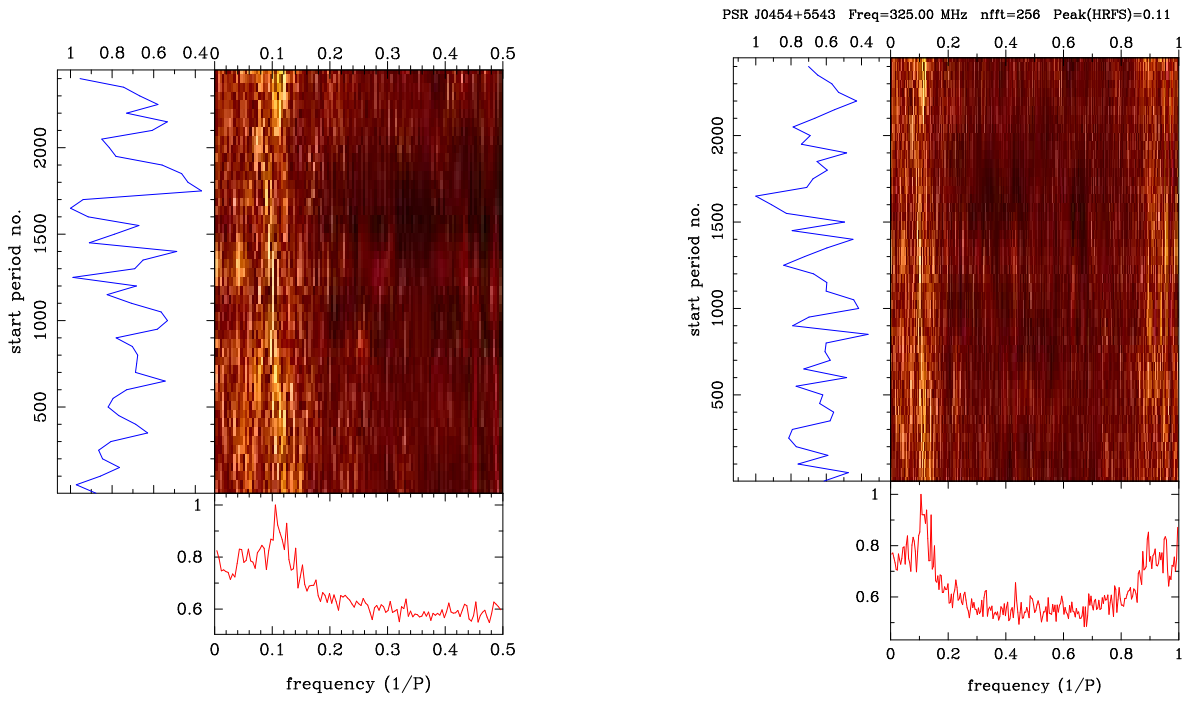


Fig. 30.— PSR B0450+55 : The time evolution of the LRFS (left panel) and the HRFS (right panel).

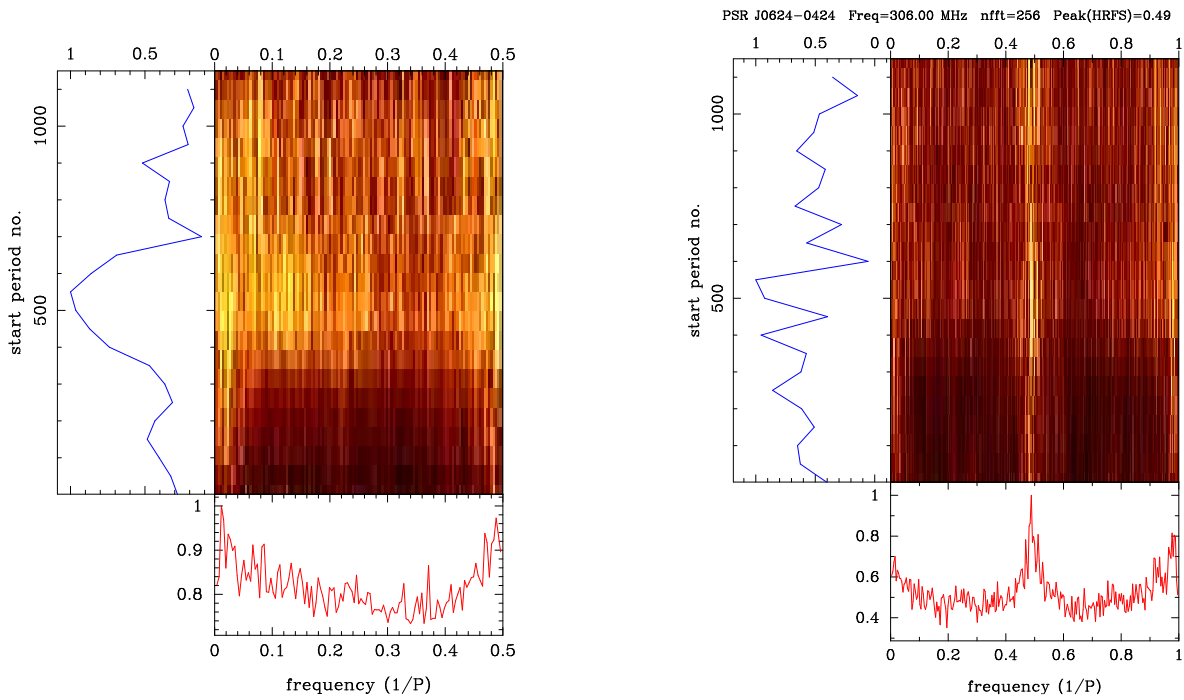


Fig. 31.— PSR B0621-04 : The time evolution of the LRFS (left panel) and the HRFS (right panel).

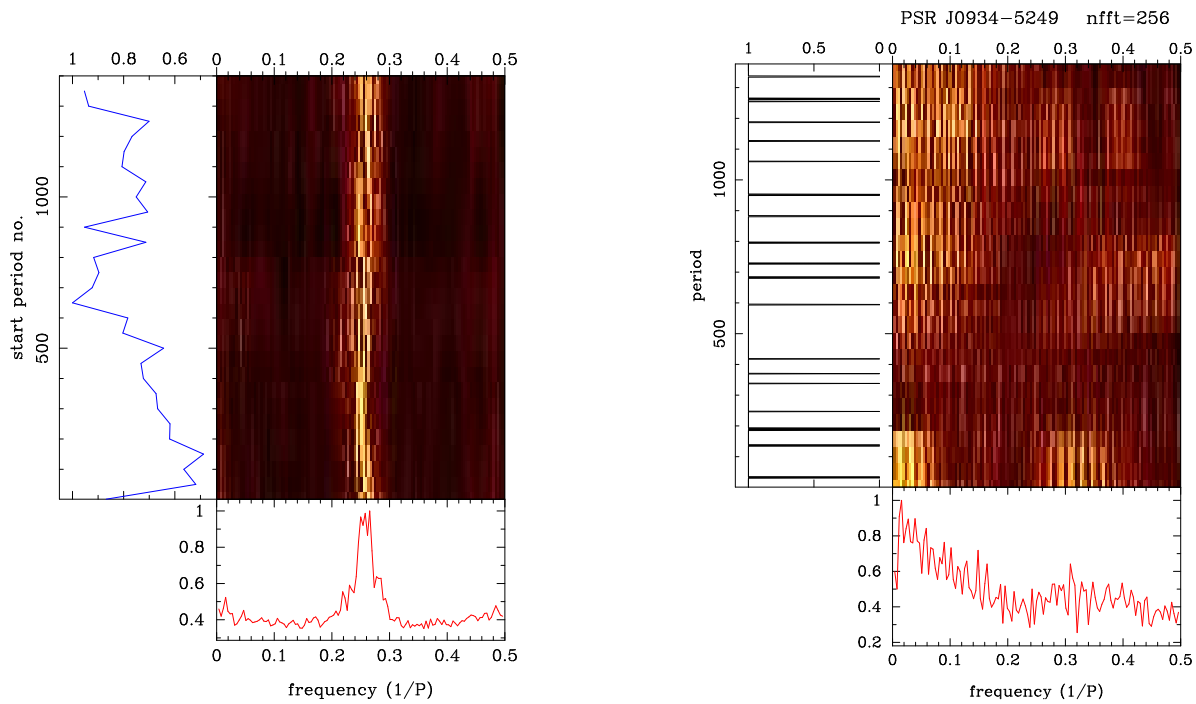


Fig. 32.— PSR B0932-52 : The time evolution of the LRFS (left panel) and the Null-Burst time series FFT (right panel).

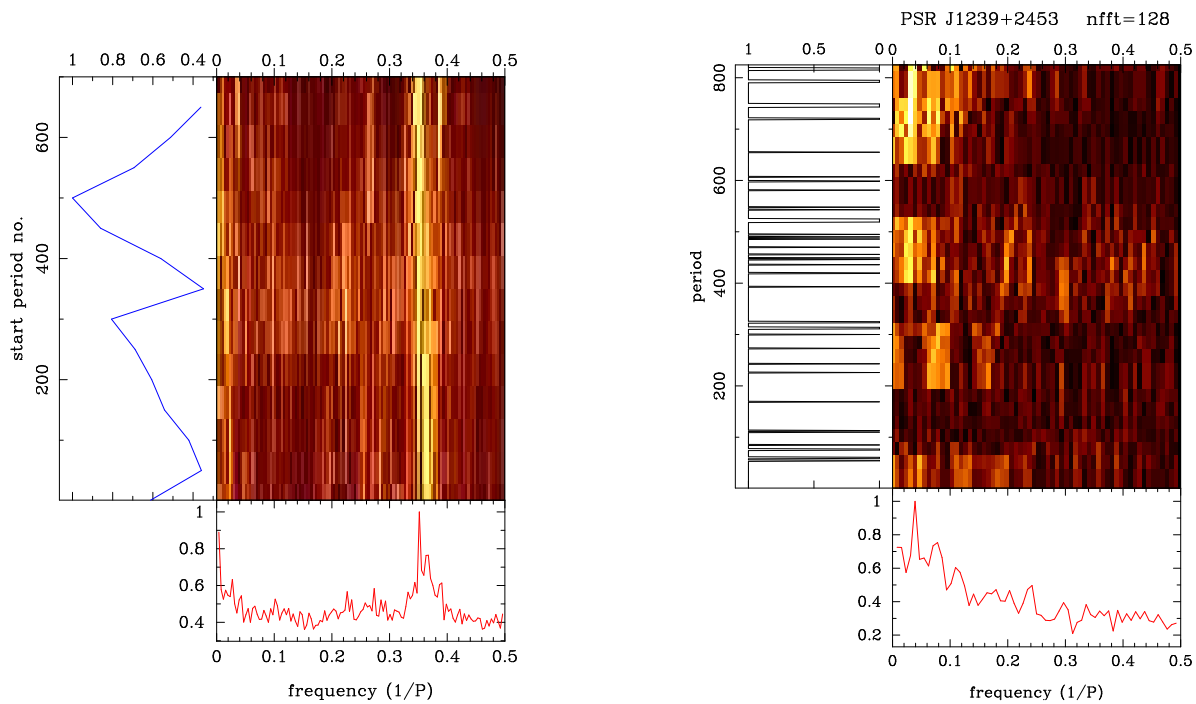


Fig. 33.— PSR B1237+25 : The time evolution of the LRFS (left panel) and the Null-Burst time series FFT (right panel).

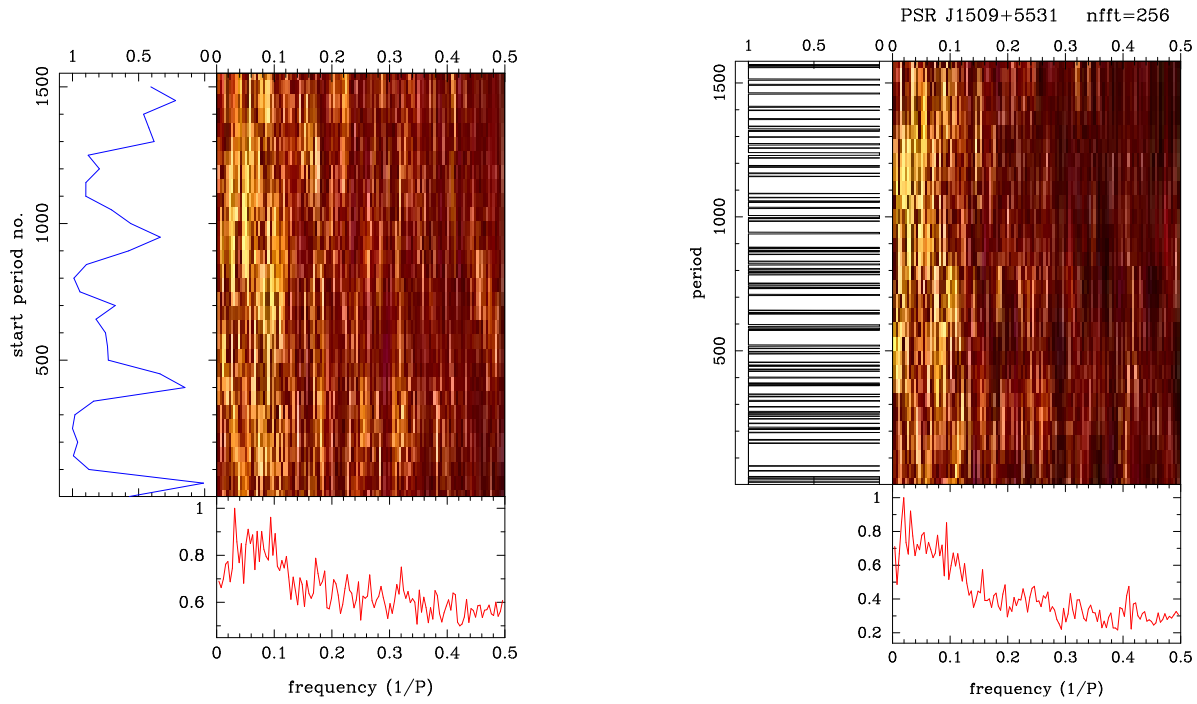


Fig. 34.— PSR B1508+55 : The time evolution of the LRFS (left panel) and the Null-Burst time series FFT (right panel).

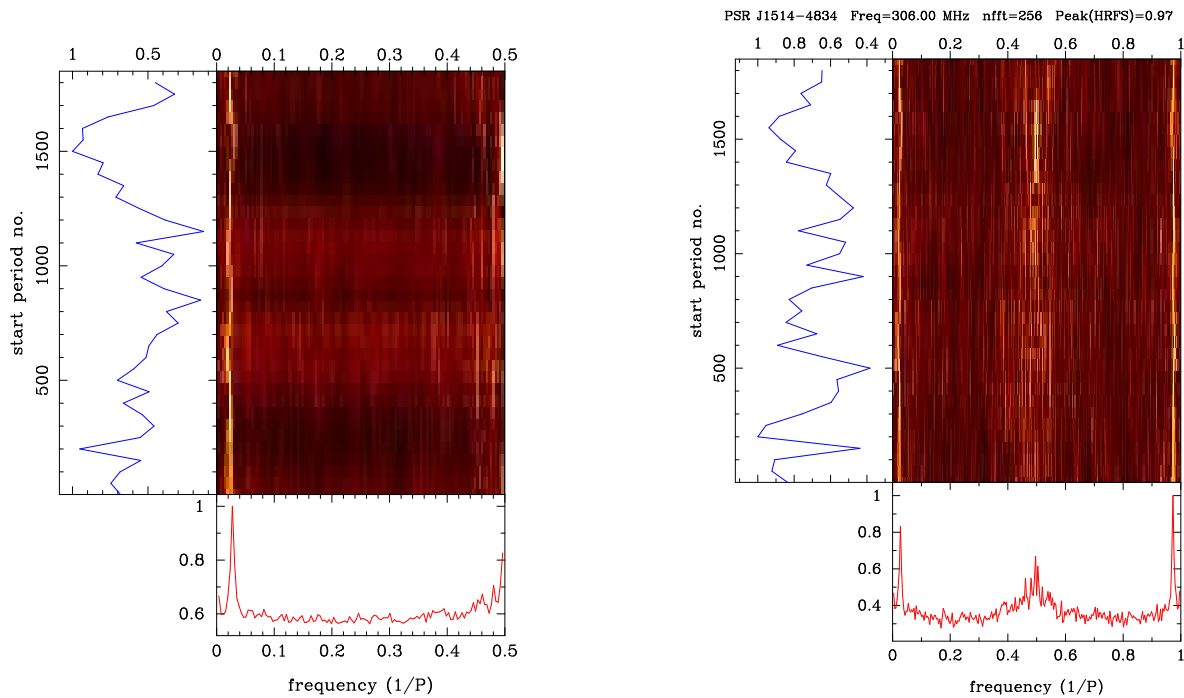


Fig. 35.— PSR B1510-48 : The time evolution of the LRFS (left panel) and the HRFS (right panel).

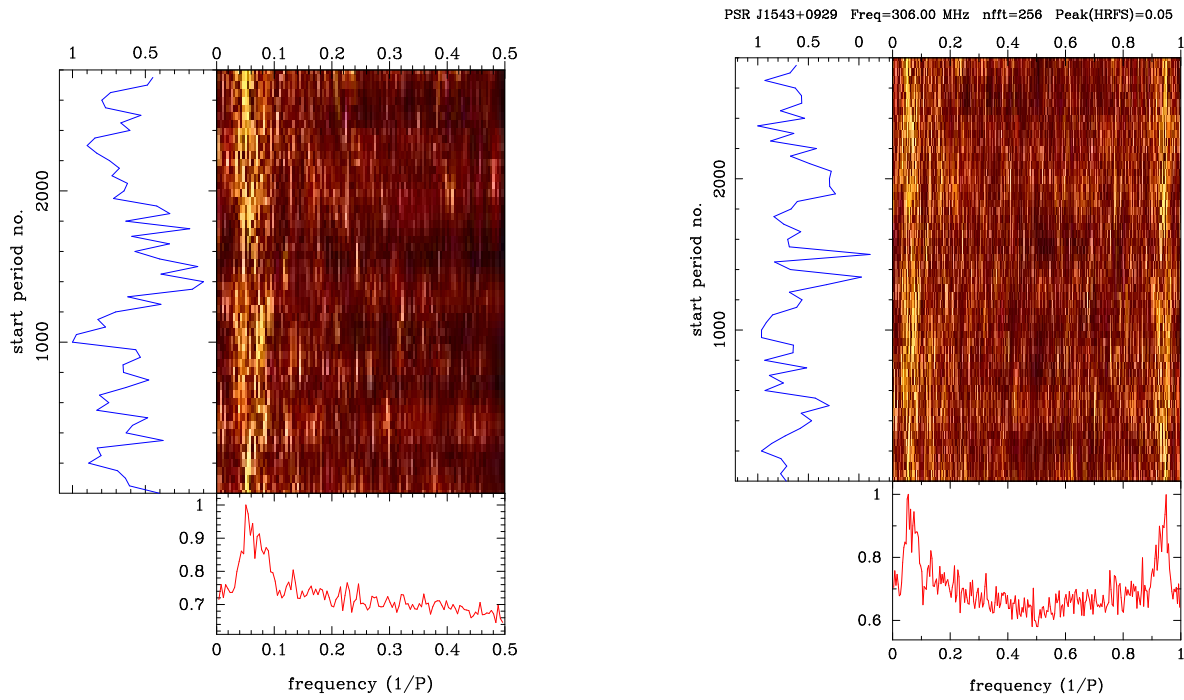


Fig. 36.— PSR B1541+09 : The time evolution of the LRFS (left panel) and the HRFS (right panel).

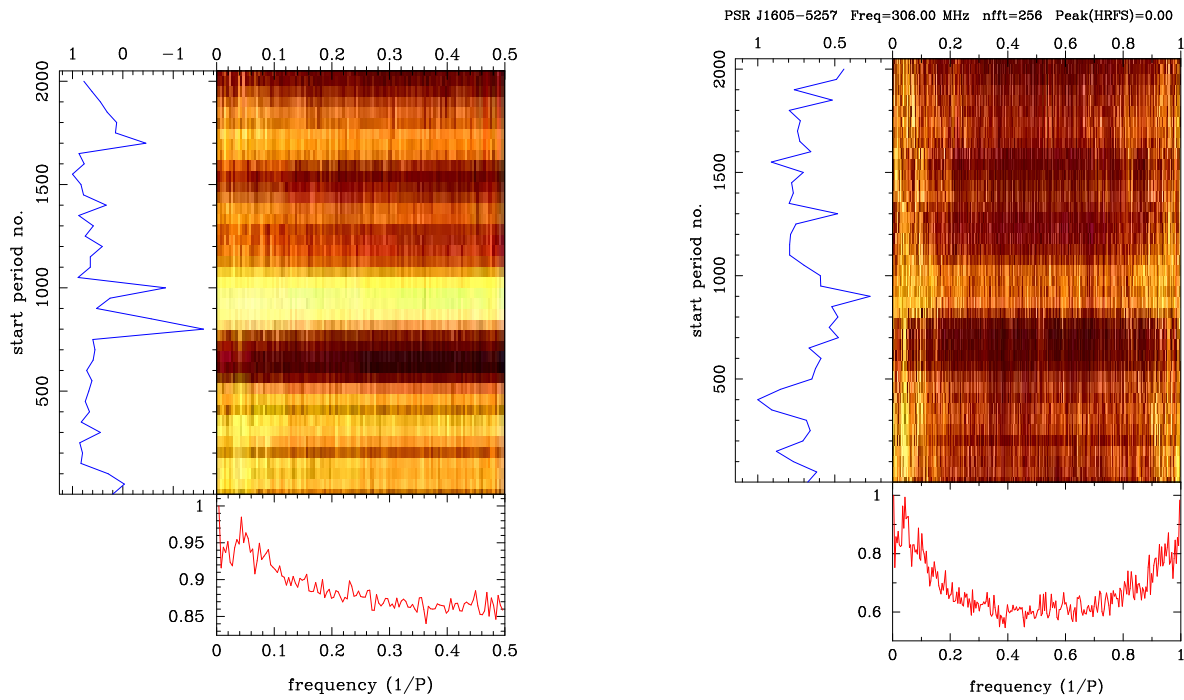


Fig. 37.— PSR B1601-52 : The time evolution of the LRFS (left panel) and the HRFS (right panel).

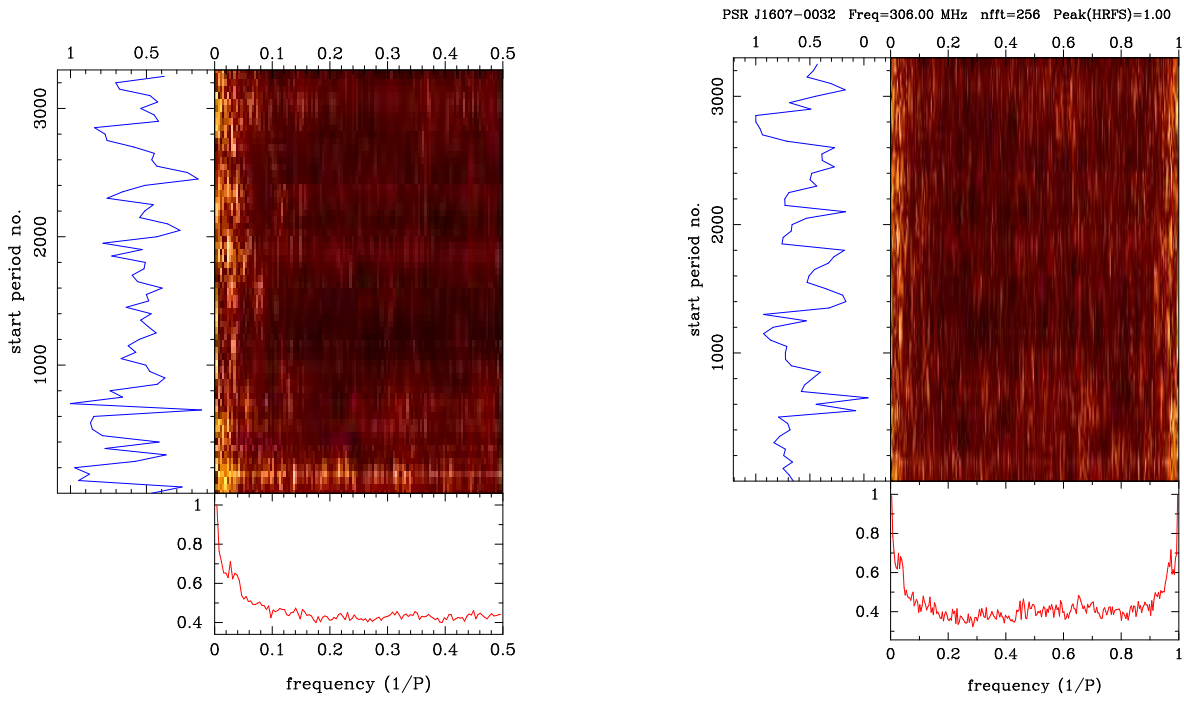


Fig. 38.— PSR B1604–00 : The time evolution of the LRFS (left panel) and the HRFS (right panel).

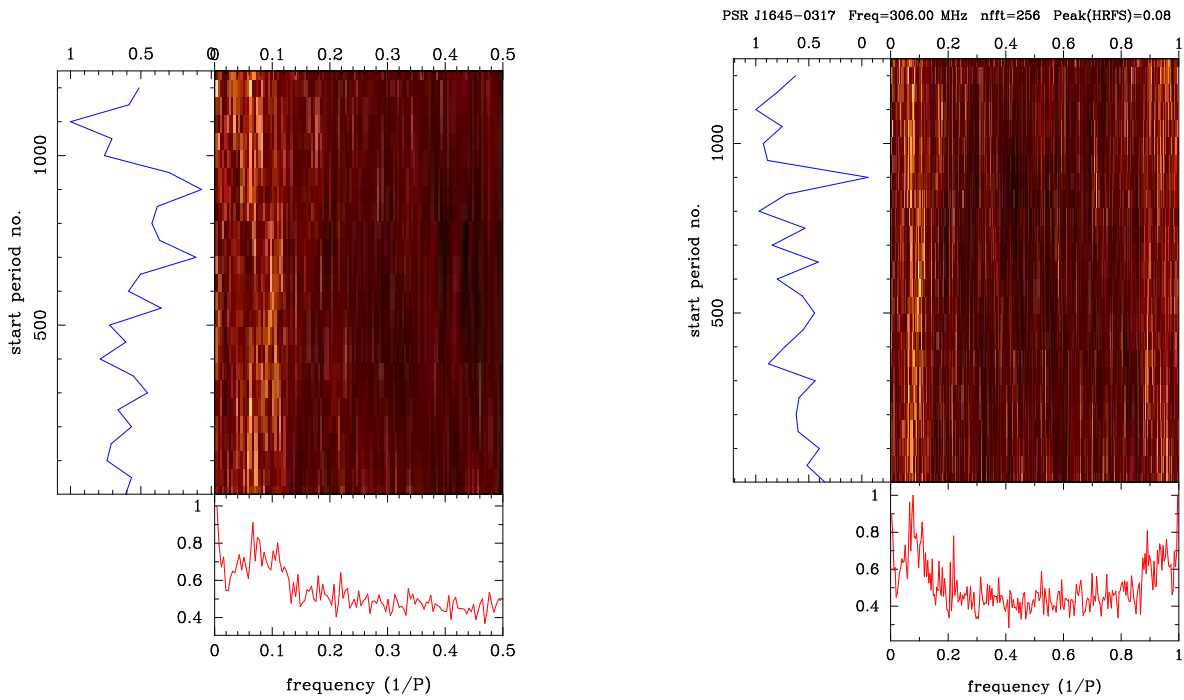


Fig. 39.— PSR B1642–03 : The time evolution of the LRFS (left panel) and the HRFS (right panel).

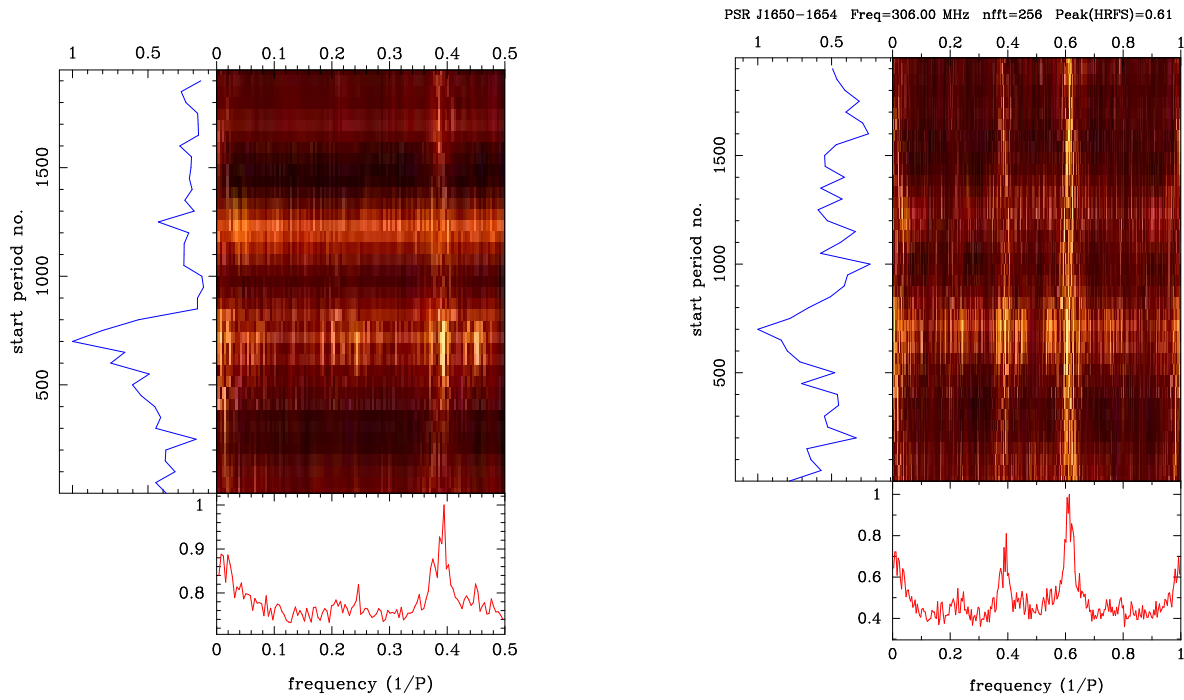


Fig. 40.— PSR J1650–1654 : The time evolution of the LRFS (left panel) and the HRFS (right panel).

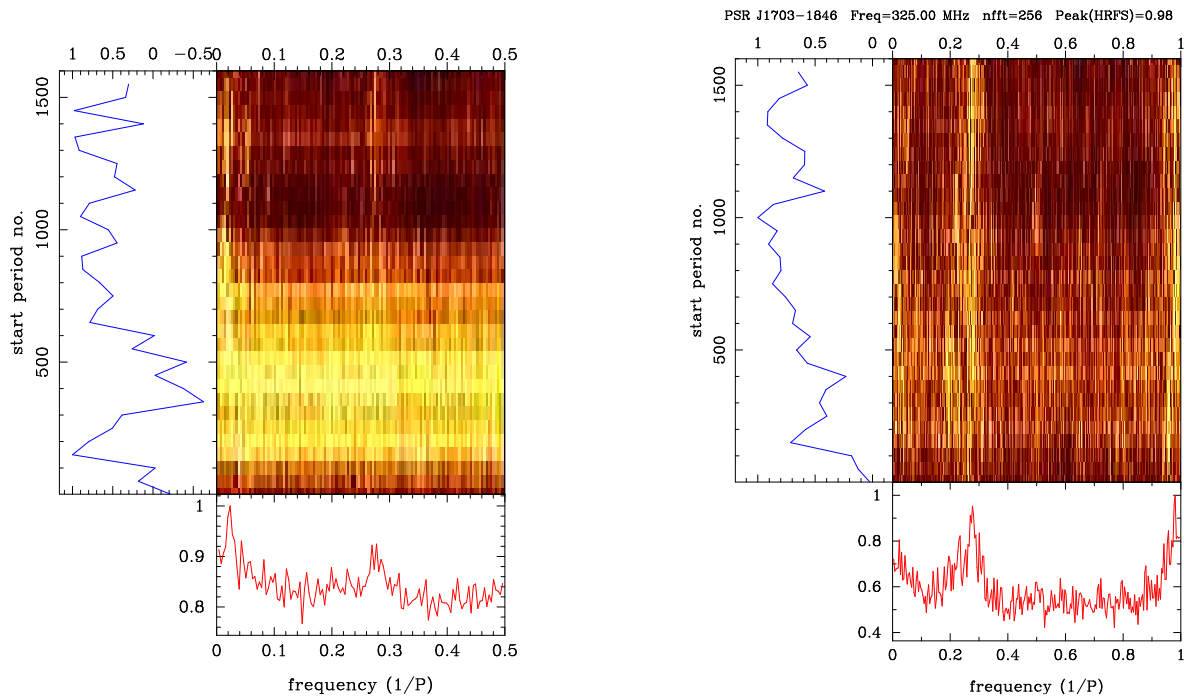


Fig. 41.— PSR B1700–18 : The time evolution of the LRFS (left panel) and the HRFS (right panel).

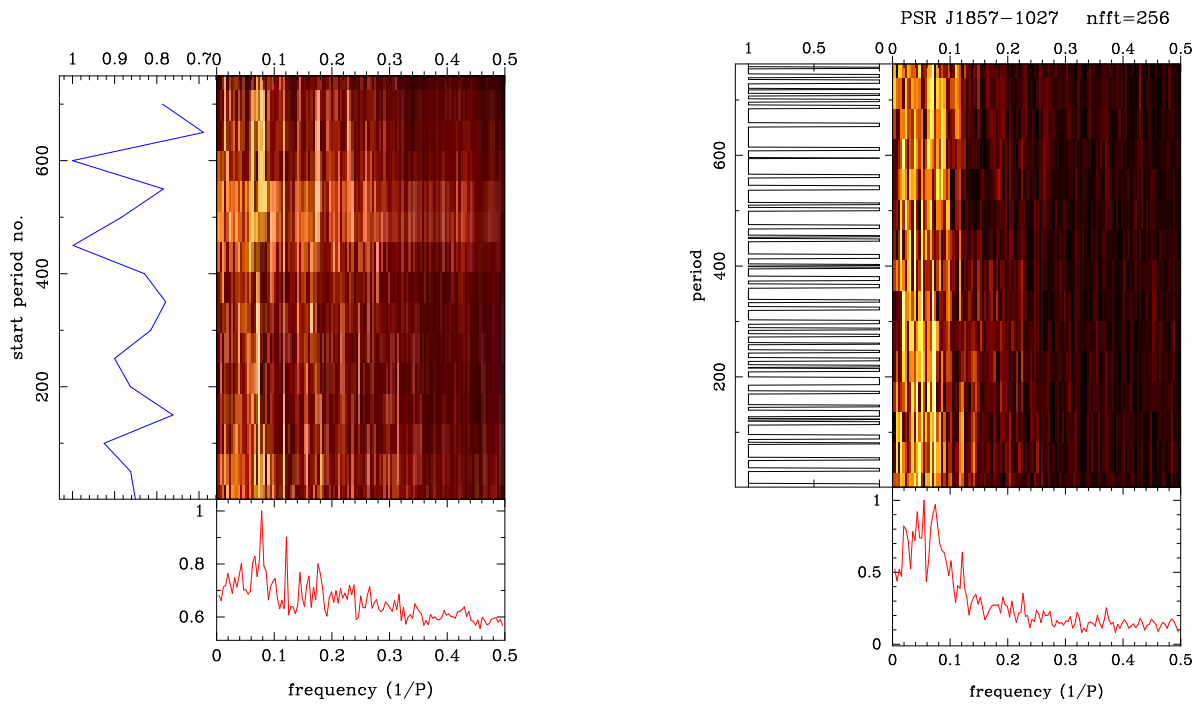


Fig. 42.— PSR J1857-1027 : The time evolution of the LRFS (left panel) and the Null-Burst time series FFT (right panel).

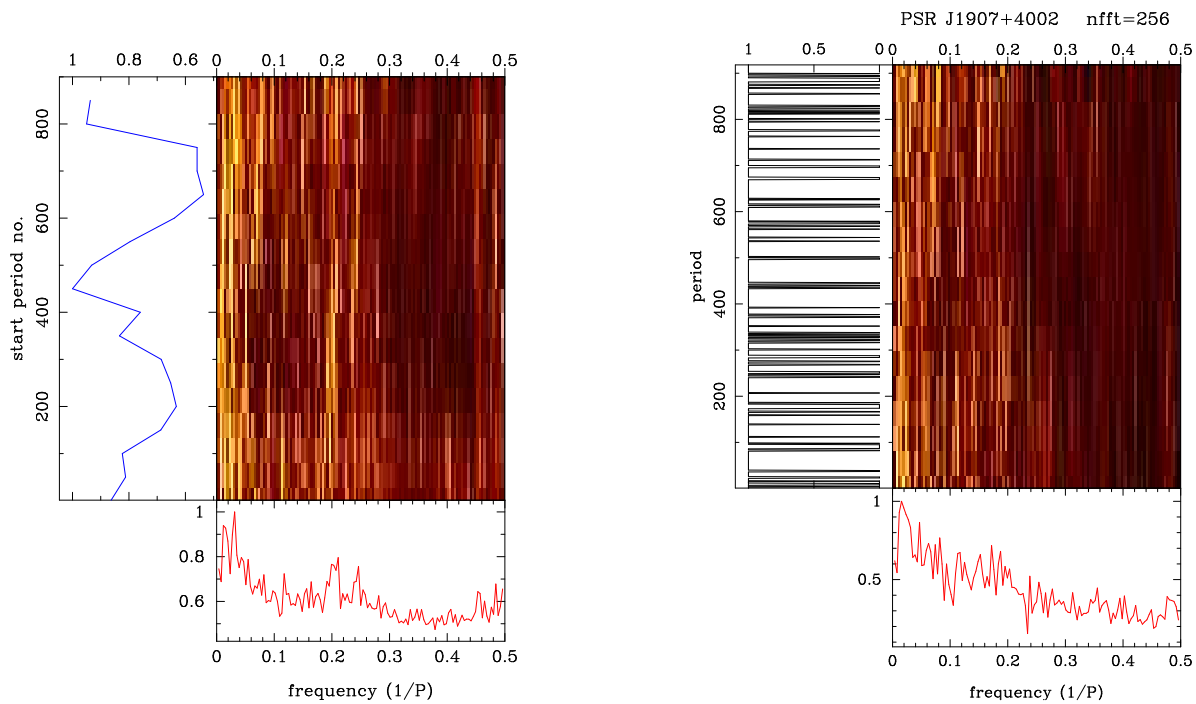


Fig. 43.— PSR B1905+39 : The time evolution of the LRFS (left panel) and the Null-Burst time series FFT (right panel).

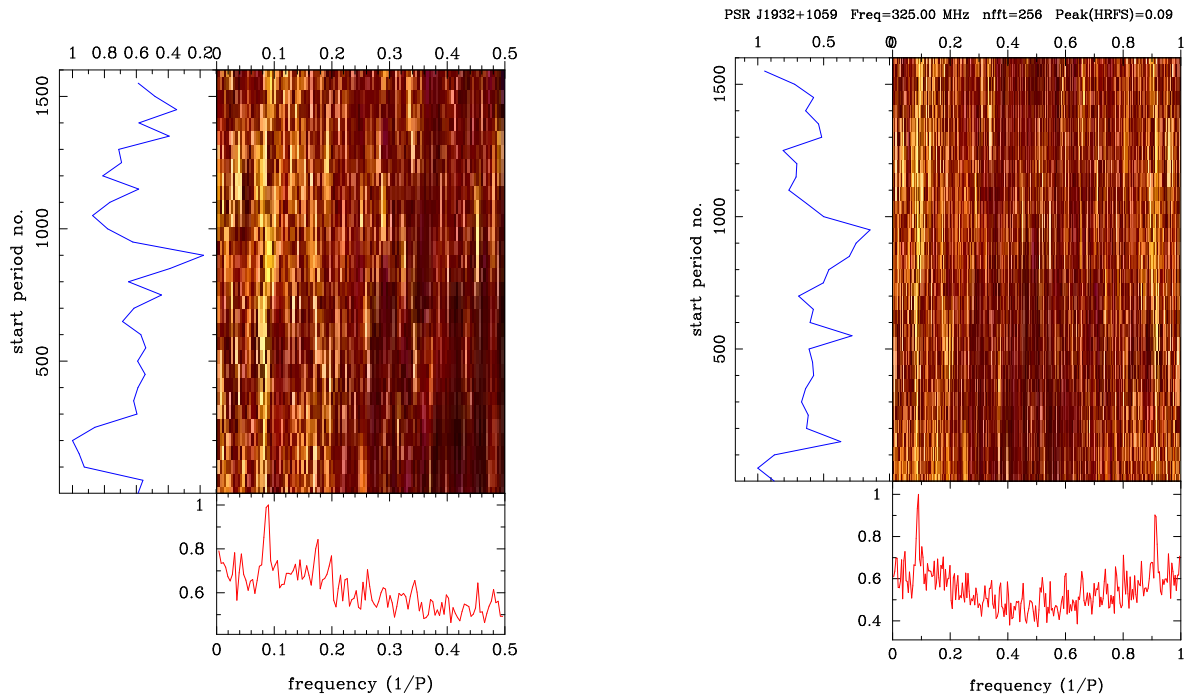


Fig. 44.— PSR B1929+10 : The time evolution of the LRFS (left panel) and the HRFS (right panel).

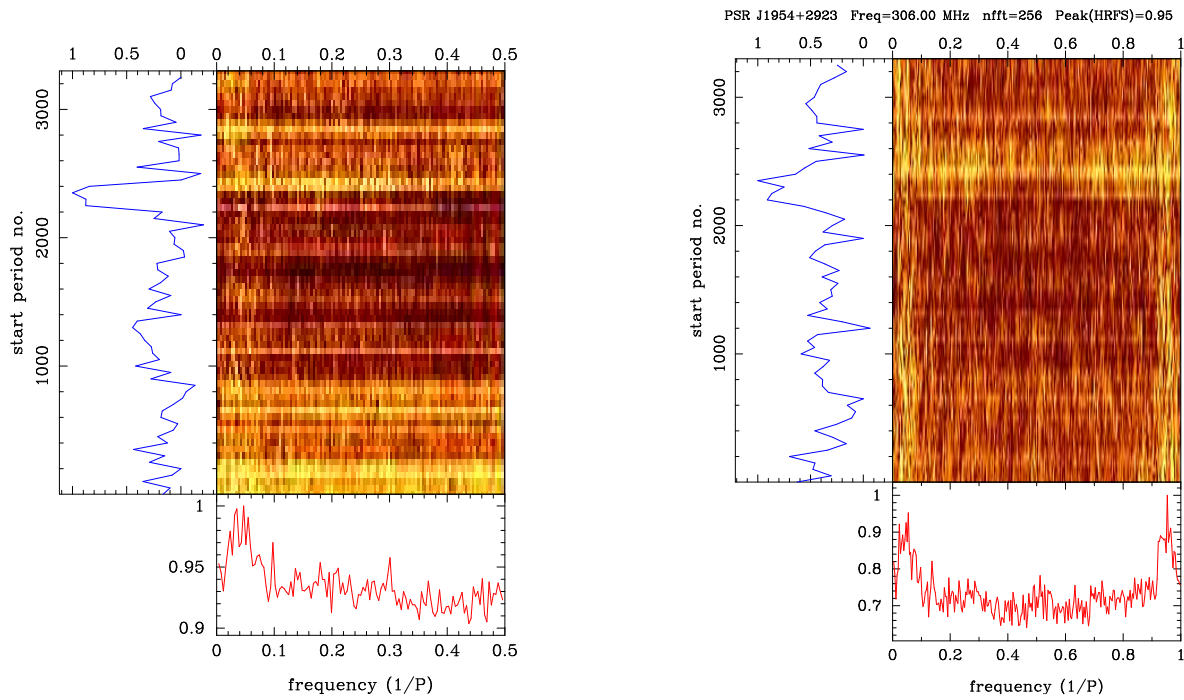


Fig. 45.— PSR B1952+29 : The time evolution of the LRFS (left panel) and the HRFS (right panel).

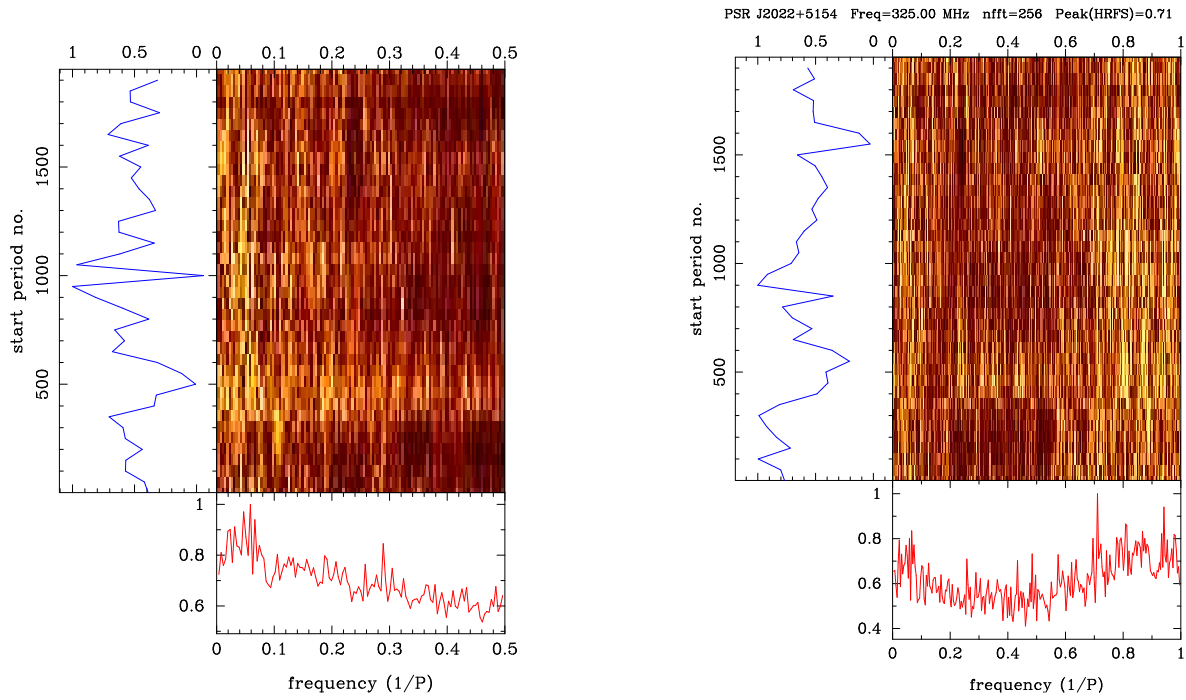


Fig. 46.— PSR B2021+51 : The time evolution of the LRFS (left panel) and the HRFS (right panel).

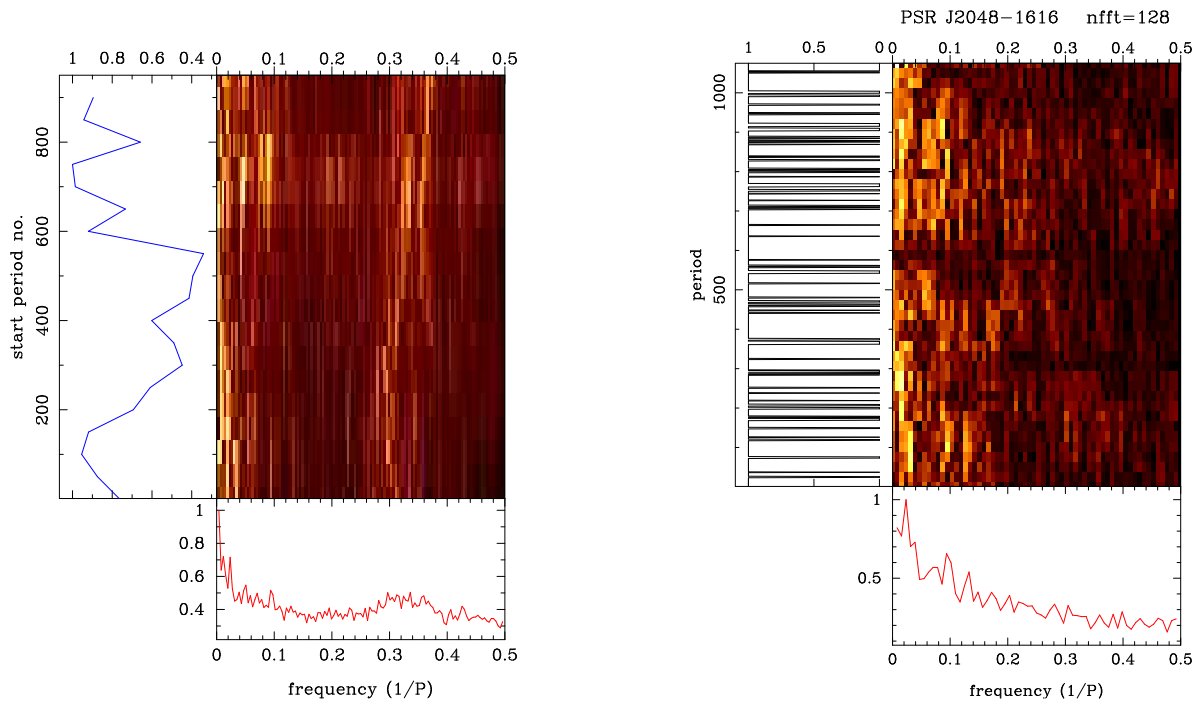


Fig. 47.— PSR B2045-16 : The time evolution of the LRFS (left panel) and the Null-Burst time series FFT (right panel).

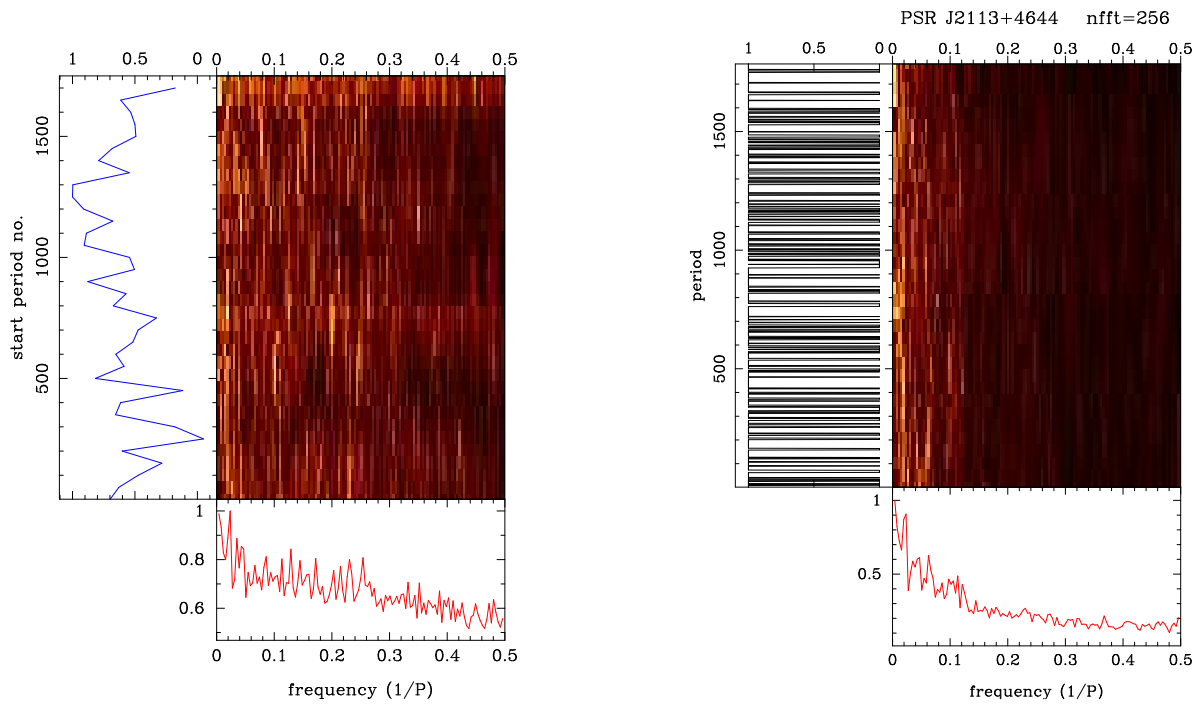


Fig. 48.— PSR B2111+46 : The time evolution of the LRFS (left panel) and the Null-Burst time series FFT (right panel).

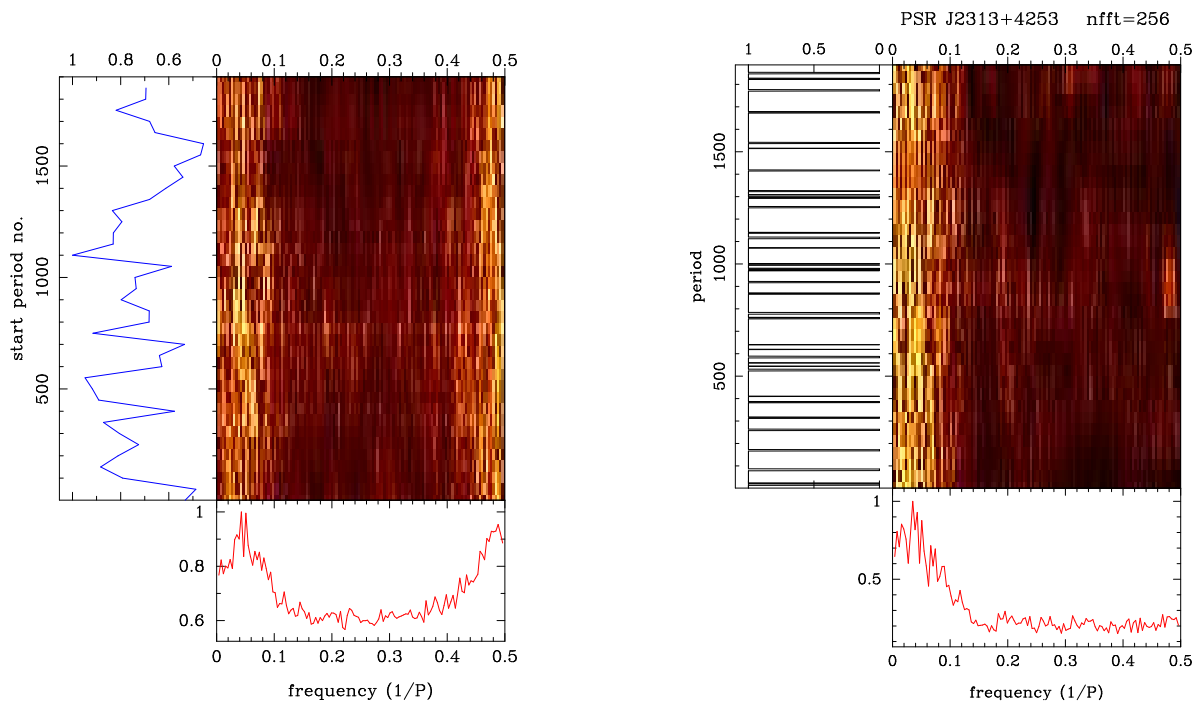


Fig. 49.— PSR B2310+42 : The time evolution of the LRFS (left panel) and the Null-Burst time series FFT (right panel).

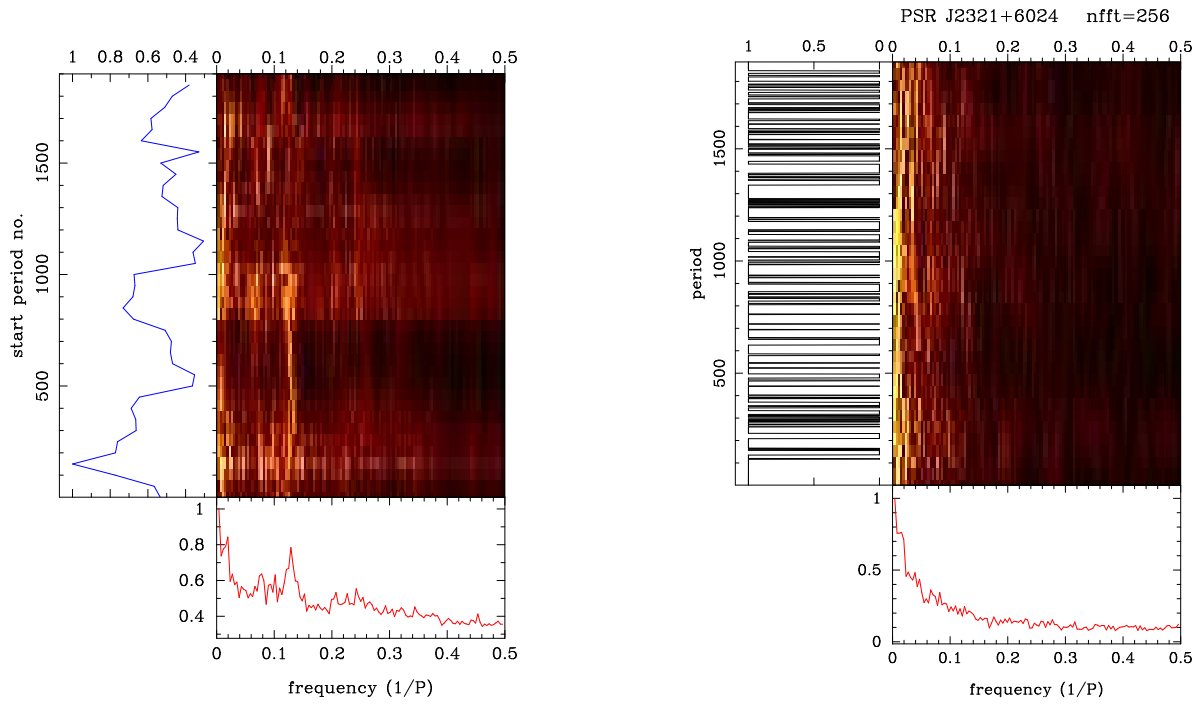


Fig. 50.— PSR B2319+60 : The time evolution of the LRFS (left panel) and the Null-Burst time series FFT (right panel).

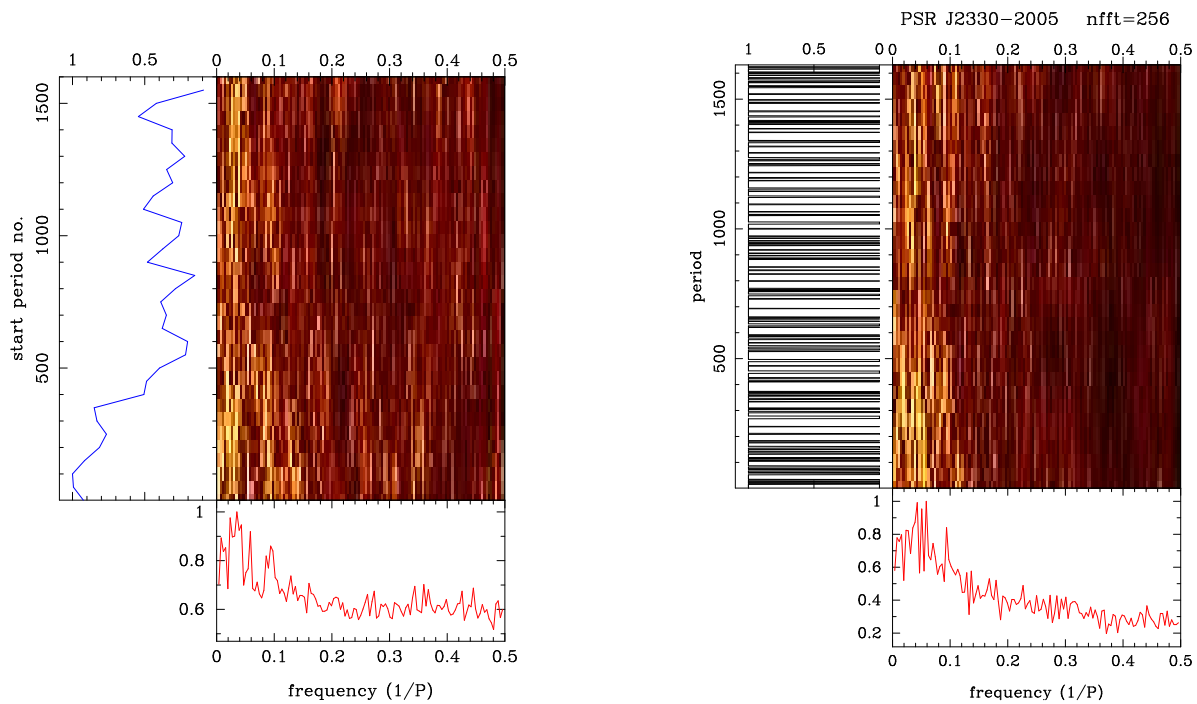


Fig. 51.— PSR B2327-20 : The time evolution of the LRFS (left panel) and the Null-Burst time series FFT (right panel).